ELEMENTA
Science of the Anthropocene

Akino, R, et al. 2024. Characteristics of late summer Arctic brash sea ice and its melting effect on the surface-water biogeochemistry of the Chukchi Shelf and Canada Basin. *Elem Sci Anth*, 12: 1. DOI: https://doi.org/10.1525/elementa.2023.00094

RESEARCH ARTICLE

# Characteristics of late summer Arctic brash sea ice and its melting effect on the surface-water biogeochemistry of the Chukchi Shelf and Canada Basin

Ryota Akino[1,*], Daiki Nomura[1,2,3], Reishi Sahashi[1], Manami Tozawa[1], Mariko Hatta[4], Kohei Matsuno[1,3], Wakana Endo[1], Takuhei Shiozaki[5], Tatsuya Kawakami[1], Masato Ito[6], Akihiko Murata[4], and Amane Fujiwara[4]

To understand the impact of the melting of late summer Arctic brash ice on the surface waters of the Chukchi Sea, we collected sea-ice samples during 2021. Floating sea ice was collected by a wire mesh pallet cage from the side of the R/V *Mirai*. We measured physical and biogeochemical parameters such as salinity, oxygen stable isotopic ratios, turbidity, and concentrations of chlorophyll-a and nutrients. The samples of brash ice were multiyear ice based on satellite back-trajectory analysis. Comparison of nutrient concentrations in brash ice with those of seawater samples from the temperature minimum layer similar to the water in the sea ice originated suggested that the characteristics of the brash ice were greatly affected by biogeochemical processes such as remineralization. The extremely high turbidity and concentrations of chlorophyll-a observed in the brown/green ice samples reflected the impact of sediment as well as the influence of biological activities. The N:P ratios were less than 1 because of the high phosphate concentrations, even though the ammonium concentrations were high. We hypothesized that this low N:P ratio reflected the combined effects of the accumulation of nutrients due to remineralization in the biofilm and differences of remineralization rate and adsorption features of nitrogen and phosphorus. Based on the high nitrate and ammonium concentrations in the sea-ice samples, we postulated a marked impact of sea-ice meltwater on the nitrogen cycle in the nitrate-depleted surface waters of the Chukchi Sea during late summer. We estimated that meltwater nitrogen could support 0.3%–2.6% of primary production in the northern Chukchi Sea. Our results suggest that high-turbidity ice will play an important role as a source of nutrients to the ocean during melting of sea ice, and understanding its distribution, amount, and geochemical characteristics is vital.

**Keywords:** Sea ice, Brash ice, Melting process, Remineralization, Chukchi Sea, Arctic Ocean

## 1. Introduction

The Chukchi Sea, located north of Bering Strait, is in an area of high primary production (Springer and McRoy, 1993; Gosselin et al., 1997; Hill and Cota, 2005). The Alaska Coastal Current, which is oligotrophic, flows into the Chukchi Sea along the eastern side of Bering Strait (Walsh et al., 1989; Hansell and Goring, 1990). The nutrient-rich Anadyr Current from the west (McRoy, 1993; Springer and McRoy, 1993) and freshwater from the Yukon River and other rivers from the east (Aagaard et al., 2006; Spencer et al., 2008) also enter through the Bering Strait. Although the Chukchi Sea therefore has complex nutrient supply pathways, nitrate depletion occurs in summer and limits primary production (Cota et al., 1996; Nishino et al., 2016). In addition, large amounts of organic matter produced during blooms reach and are decomposed at the seafloor, creating an anoxic environment in the sediments that favors the further loss of nitrate through denitrification (Brown et al., 2015).

The Arctic Ocean, including the Chukchi Sea, is characterized by extensive sea ice in winter (Comiso, 2010). Sea ice forms when seawater freezes, with biological materials from seawater becoming trapped in brine channels and pockets within the ice matrix (Petrich and Eicken, 2010).

[1] Graduate School/Faculty of Fisheries Sciences, Hokkaido University, Hakodate, Hokkaido, Japan
[2] Field Science Center for Northern Biosphere, Hokkaido University, Hakodate, Hokkaido, Japan
[3] Arctic Research Center, Hokkaido University, Sapporo, Hokkaido, Japan
[4] Japan Agency for Marine-Earth Science and Technology (JAMSTEC), Yokosuka, Japan
[5] Atmosphere and Ocean Research Institute, The University of Tokyo, Kashiwa, Chiba, Japan
[6] National Institute of Polar Research, Tachikawa, Tokyo, Japan

* Corresponding author:
Email: r.akino@eis.hokudai.ac.jp

At the growing ice front with high brine volume, brine expulsion drives nutrients from sea ice to ocean (Griewank and Notz, 2013). As sea ice thickens and brine volume decreases below 5% in its colder portions, sea ice becomes a semi-enclosed system (Golden et al., 1998; Pringle et al., 2009; Zhou et al., 2013). The exchange of solutes between brine and seawater when driven only by diffusion is a very slow process (Notz and Worster, 2009). Within a semi-enclosed brine system, changes to sea-ice nutrients are thus driven by biological processes (Thomas et al., 2010). In other words, nutrient stocks in sea ice are driven by a combination of thermodynamic and biological processes. In the Northern Hemisphere, including the Arctic Ocean, snowfall has also been reported to be an important source of nitrate and ammonium (Kaartokallio, 2001; Granskog et al., 2003; Krell et al., 2003; Nomura et al., 2010; Nomura et al., 2011). For example, Granskog et al. (2003) found considerably higher concentrations of dissolved inorganic nitrogen in snow and snow-influenced sea ice than in the underlying sea ice column. Dust and bushfires are also major sources of nutrients to the Arctic, especially nitrate (Zhang et al., 2020; Ardyna et al., 2022).

The nutrients left in sea ice at the end of the ice-growing season are released into surface seawater as the melting season begins (Tovar-Sánchez et al., 2010). At the same time, a phytoplankton bloom, specific to the sea-ice-covered region, occurs at and near the margin of the ice cover as light intensity increases under the ice (Niebauer et al., 1995; Arrigo et al., 2012). Sea ice thus supports ecosystems inside and outside of the ice and plays an important role in the formation of these marine ecosystems. Nutrient-rich sea ice may fertilize the ocean when it melts. Especially in recent years, there has been a significant decrease in multiyear ice in the Arctic Ocean (Serreze et al., 2019), and the melting of multiyear ice, significantly affected by snow cover and organic degradation processes (Sahashi et al., 2022), may affect nutrient cycling in the Arctic in the future. Furthermore, in the Chukchi/Beaufort Sea shelf region of the Arctic Ocean, sea ice (pack ice) generally moves from east to west while ocean currents flow from west to east (de Vernal et al., 2005). Sea ice can thus transport nutrients from one region to another both temporally and spatially. The biogeochemical composition of sea ice and a comparison of nutrient concentrations in sea ice and seawater are therefore subjects of great interest.

Ice algae inhabit sea ice, where they can take advantage of nutrients (Thomas et al., 2010). Ice algae support the reproduction of higher trophic organisms such as zooplankton and fish and play an important role in the Arctic marine ecosystem (Kohlbach et al., 2016). In addition, sea ice sometimes contains bottom sediments such as sand and organic matter (Eicken et al., 2005; Nomura et al., 2010; Waga et al., 2022). In such environments with a high biomass of ice algae, the "sea ice-nutrient paradox" (e.g., Arrigo et al., 1995; Roukaerts et al., 2021) may occur. This phenomenon is characterized by a simultaneous increase of biomass and nutrients. Ice algae, known to secrete extracellular polymeric substances (EPS; Krembs et al., 2011), have been suggested to aggregate in biofilms that are responsible for this behavior (Roukaerts et al., 2021); however, our understanding of biofilms in the biogeochemistry of sea ice is currently limited.

Arctic sea-ice studies have generally focused on the collection of ice cores from large sea-ice floes accessed by research vessel (e.g., Werner et al., 2007; Nicolaus et al., 2022) or fast ice accessed from land (Krembs et al., 2002; Zhou et al., 2013). Brash ice, defined as floating ice composed of broken-up pieces <2 m wide (World Meteorological Organization, 1970), is rarely collected from research vessels or from land. Brash ice encountered during summer is the remnant of sea ice that did not melt and is thought to be nearly a year old or even older. Such brash ice is likely to have undergone various processes that would have changed its biogeochemical properties.

Nomura et al. (2023b) conducted a study that focused on the biogeochemistry of brash ice in the Southern Ocean. They compared brash-ice with sea-ice core data and discussed the seasonal changes in the biogeochemical composition of brash ice and the dynamics of brash ice from a biogeochemical point of view. However, there have been no studies of brash ice in the Arctic Ocean. The melting of sea ice has been progressing dramatically in the Arctic Ocean in recent years (Stroeve and Notz, 2018). Describing and evaluating the characteristics of brash ice is important, as brash ice represents the final stage in the melting of summer sea ice, with the greatest impact on the ocean surface layer.

In this study, we collected brash ice in the northern Chukchi Sea during cruise MR21-05C of the R/V *Mirai* in 2021. After melting the ice, we measured concentrations of nutrients and chlorophyll-a as well as physical properties such as salinity, oxygen stable isotope ratios, and turbidity. We compared these properties with those of fall and winter seawater, from which sea ice is formed. We considered physical processes such as brine discharge and seawater exchange as well as biogeochemical processes such as primary production and the decomposition of organic matter. We also compared our data with first-year ice core data (Deming et al., 2020) collected offshore near Utqiaġvik (Barrow), Alaska. In addition, based on the nutrient concentrations of brash ice measured in this study, we estimated the contribution of nutrients supplied from sea ice to primary production in the Chukchi Sea and Canadian Basin.

## 2. Materials and methods

### *2.1. Sampling and treatment of samples*

Brash sea ice, seawater, and snow samples were collected during cruise MR21-05C of the R/V *Mirai* from August 31 to October 21, 2021, in the Pacific sector of the Arctic Ocean, the northern Bering Sea, and the North Pacific Ocean under the framework of the Arctic Challenge for Sustainability II (ArCS II) Project (**Figure 1** and **Table 1**). The sea-ice samples (less than 1 $m^3$) were collected at three sites, stations ICE1, ICE3, and ICE4, using a wire mesh pallet cage (1.2 m × 1.0 m × 0.9 m) connected to the ship's crane (Figure S1). Five, one, and two brash-ice samples were collected at stations ICE1, ICE3, and ICE4,

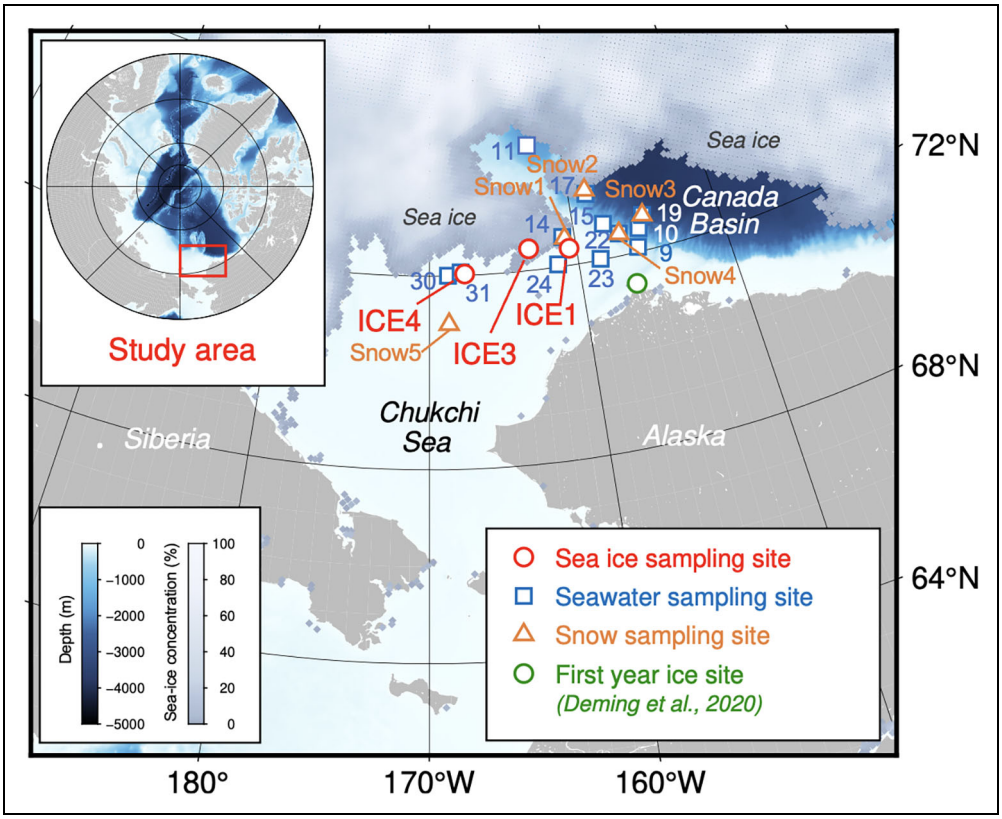


**Figure 1. Location map of the study area and sampling sites.** Mean values of sea-ice concentrations during the MR21-05C cruise (from August 31 to October 21, 2021) are depicted based on the satellite image (CryoSat-2). Data from the ice-coring site were obtained by Deming et al. (2020) from two core samples collected at 71.29°N, 156.72°W and 71.37°N, 156.51°W in May 2017.

respectively (Table S1). The temperature of the ice (outside and inside) samples was measured on the deck of the ship with a temperature probe (Testo 110 NTC, Brandt Instruments, Inc., USA) immediately after the sea-ice sampling. Each sample of ice was cut with a saw on the deck of the ship, and then the temperature of the inside of the ice was measured. After the temperature measurement, the ice was cut into small cubes (0.15 m × 0.15 m × 0.15 m) in a cold room (−15°C), and sample ID# was attached to each small cube (Table S1). Each sea-ice cube was then melted in a gas-tight plastic bag (AAK10, GL Science, Japan) under dark, cool conditions (4°C).

Samples of snow fallen during the cruise were collected over the clean snow tray (1.0 m × 1.0 m) on the deck of R/V *Mirai* after the snowfall event. The samples were collected manually with clean rubber gloves and placed into Ziploc® bags. The snow samples were then allowed to melt in the dark under cool conditions (4°C).

The meltwater samples were subsampled into: (1) 10 mL polyethylene screw-cap vials (Eiken Chemical Co. Ltd., Tokyo, Japan) to measure concentrations of the nutrients $NO_3^-$, $NO_2^-$, $NH_4^+$, $PO_4^{3-}$, and $Si(OH)_4$, after being filtered through a 0.22 µm Durapore polyvinylidene fluoride membrane filter (MILLEX GV Filter unit, Merck Millipore Ltd., Germany); (2) 15 mL glass, screw-cap vials (Nichiden-Rika Glass Co. Ltd., Kobe, Japan) for $\delta^{18}O$ determinations; (3) 300 or 500 mL Nalgene polycarbonate bottles (Thermo Fisher Scientific Inc., Waltham, MA, USA) for chlorophyll-a (chl-a) measurements; and (4) 1 L Nalgene polycarbonate bottles (Thermo Fisher Scientific Inc., Waltham, MA, USA) with 1% glutaraldehyde for microscopic examination. Samples for chl-a measurements were immediately filtered onto 25 mm Whatman GF/F filters. Pigments on the filters were extracted with dimethyl formamide (Suzuki and Ishimaru, 1990) for 24 h.

Surface seawater samples at a depth of 5 m and winter water from the temperature minimum layer (TML), the depth at which the water temperature reached a minimum, were collected from vertical profiles in rosette-mounted, 10 L Niskin bottles (Ocean Test Equipment, Inc., Lauderdale, FL, USA). Seawater was subsampled in the same manner as the meltwater. Vertical profiles of temperature and salinity were measured with a conductivity–temperature–depth probe (SBE 9 plus, Sea-Bird Electronics, Bellevue, WA, USA).

### *2.2. Sample analysis*

The salinity of meltwater samples was measured with a conductivity sensor (Cond 315i, WTW, Germany). The concentrations of the nutrients $NO_3^-$, $NO_2^-$, $NH_4^+$, $PO_4^{3-}$, and $Si(OH)_4$ in meltwater and seawater were determined in accordance with the Joint Global Ocean Flux Study (JGOFS) spectrophotometric method (JGOFS, 1994) using an autoanalyzer (QuAAtro 2-HR system; BL-tec, Osaka, Japan). The analyzer was calibrated with reference materials for nutrient analysis (CRMs, Lot: CE, CL, CO, CG; KANSO

**Table 1. Station, location, and date of sampling for brash sea ice, seawater, and snow during cruise MR21-05C**

| Station | Longitude (W) | Latitude (N) | Date in 2021 | Water Depth (m)[a] | Type of Sampling |
|---|---|---|---|---|---|
| ICE1 | 160°29 | 72°21 | Sep 17 | —[a] | Sea ice |
| ICE3 | 163°13 | 72°27 | Sep 22 | — | Sea ice |
| ICE4 | 167°38 | 72°02 | Sep 23 | — | Sea ice |
| 9 | 155°55 | 72°06 | Sep 13 | 209 | Vertical water (TML[b] detected) |
| 10 | 155°35 | 72°28 | Sep 14 | 1829 | Vertical water (TML detected) |
| 11 | 161.56 | 74°31 | Sep 15 | 1688 | Vertical water (TML detected) |
| 14 | 160°50 | 72°36 | Sep 17 | 49 | Vertical water |
| 15 | 157°55 | 72°43 | Sep 18 | 377 | Vertical water (TML detected) |
| 17 | 158°43 | 73°24 | Sep 18 | 2214 | Vertical water (TML detected) |
| 19 | 155°08 | 72°43 | Sep 19 | 2969 | Vertical water (TML detected) |
| 22 | 156°59 | 72°28 | Sep 20 | 466 | Vertical water TML detected) |
| 23 | 158°32 | 72°01 | Sep 21 | 56 | Vertical water |
| 24 | 161°23 | 72°03 | Sep 21 | 31 | Vertical water |
| 30 | 168°45 | 72°00 | Sep 23 | 51 | Vertical water |
| 31 | 167°54 | 72°04 | Sep 23 | 50 | Vertical water |
| Snow1 | 160°41 | 72°34 | Sep 17 | — | Snow |
| Snow2 | 158°45 | 73°29 | Sep 18 | — | Snow |
| Snow3 | 155°08 | 72°43 | Sep 19 | — | Snow |
| Snow4 | 156°59 | 72°28 | Sep 20 | — | Snow |
| Snow5 | 168°45 | 71°00 | Sep 25 | — | Snow |

[a]For vertical water sampling sites; no data (—) for other sites.

[b]Temperature minimum layer (TML).

Technos Co., Ltd., Japan). Detection limits (DL) for the nutrient analyses were 0.03 μmol $L^{-1}$ for $NO_3^-$, 0.005 μmol $L^{-1}$ for $NO_2^-$, 0.04 μmol $L^{-1}$ for $NH_4^+$, 0.010 μmol $L^{-1}$ for $PO_4^{3-}$, and 0.10 μmol $L^{-1}$ for $Si(OH)_4$. In this study, data below the DL were assigned a value divided by the square root of 2 for DL for further analysis and preparation of figures and tables (Croghan and Egeghy, 2003).

The $\delta^{18}O$ of meltwater and seawater samples was determined with a mass spectrometer (dual inlet mode; DELTA V Advantage, Thermo Fisher Scientific, Germany) via the equilibration method at Shoko Science Co., Ltd., Saitama, Japan. The $\delta^{18}O$ in per mil (‰) was calculated using the $^{18}O$:$^{16}O$ ratio of standard mean ocean water (SMOW) as the standard. Three kinds of working standards (DOW3: −0.07‰, AGW: −18.58‰, and SLW4: −9.62‰) were used to confirm the accuracy of the measurements.

The concentrations of chl-a were determined with a pre-calibrated fluorometer (Model-10AU; Turner Designs, Inc., Sunnyvale, CA, USA) in accordance with the method described by Welschmeyer (1994). DL for chl-a analysis was 0.01 μg $L^{-1}$. The turbidity of meltwater samples was determined with a turbidity meter (TR-55; Kasahara Chemical Instruments Corp., Saitama, Japan). The turbidity in formazin turbidity units (FTU) was determined using two kinds of polystyrene standards (10 and 100 FTU; Kasahara Chemical Instruments Corp., Saitama, Japan).

The brine volume fraction (BVF) of sea ice was calculated from the temperature and bulk salinity of sea ice following the method of Cox and Weeks (1983) for temperatures below −2°C and that of Leppäranta and Manninen (1988) for temperatures within the range 0 to −2°C. In this study, sea ice and snow samples were treated as "bulk" for each measured value.

### 2.3. Thin-section analysis

For thin-section analysis of sea ice, ice samples were sliced into subsamples 1 cm thick vertically with an electric band saw in a low-temperature room (−15°C) onboard the R/V *Mirai*. Ice sections were attached to a glass plate and cut to a thickness of about 0.1 cm with a knife. Ice crystallographic structures were photographed by illuminating the thin sections under polarized light.

### 2.4. Satellite data analysis

The distribution of sea-ice ages in our study area was obtained from Arctic Data archive System (NIPR) which was estimated from the drifting velocity of sea ice (Kimura et al., 2013) and the sea-ice concentration Bootstrap

Algorithm (Comiso, 2009; https://www.nipr.ac.jp/sea_ice/e/). Ice thicknesses and sea-ice concentrations were obtained from NASA Goddard Space Flight Center CryoSat-2 satellite observations. The data were averages of 30 days of observations and were obtained from the National Snow and Ice Data Center (2023). See Kurtz and Harbeck (2017) for more details on the data.

### 2.5. Microscopic analysis

In the land laboratory, the one-liter samples of preserved (1% glutaraldehyde) water were stored on a stone table for more than one day to allow the microprotist cells to settle to the bottom of the bottle. The samples were then concentrated to 20 mL using a syphon. Subsamples (0.5 mL) were mounted on a glass microscope slide, and diatoms were counted and identified to species level under an inverted microscope with 100–600× magnification. For species identification, we referred to Hasle and Syvertsen (1997). Diatoms, ciliates, dinoflagellates, and foraminifera were counted.

### 2.6. Snow fraction

We estimated the contribution of snow to sea ice (snow fraction) from the $\delta^{18}O$ of sea ice. For the endmembers, we used the mean $\delta^{18}O$ of TML and the mean $\delta^{18}O$ of snow. The TML endmember was corrected according to Jeffries et al. (1994; 2001). We used the following equations:

$$f_{snow} + f_{sea} = 1$$

$$f_{snow}\,\delta_{snow} + f_{sea}\,\delta_{sea} = \delta_{obs}$$

Here $f_{snow}$ and $f_{sea}$ indicate the fraction of snow and seawater, respectively; $\delta_{snow}$ and $\delta_{sea}$ indicate the endmembers of snow and seawater, respectively; and $\delta_{obs}$ indicates the $\delta^{18}O$ of the sample.

### 2.7. Estimation of impact of sea-ice melt

We examined the following calculations to quantify the impact of sea-ice melt on the surface of the Chukchi Sea. We performed separate calculations for the potential of sea-ice meltwater to alter nutrient concentrations for: (1) melting of sea ice with average nutrient concentrations, and (2) melting of high-turbidity ice (**Table 2**). We calculated how the salinity and nutrient concentrations in the mixed layer would change if melting sea ice were supplied to the oceanic mixed layer within a certain period of time. We used the nutrient concentrations of seawater in the mixed layer observed during the MR21-05C cruise as a reference for nutrient depletion and the nutrient concentrations supplied by melting sea ice during the 7 months from March to October, when the extent of sea ice is greatest. We assumed that nutrients supplied by melting sea ice during that 7-month period were not consumed and were added directly to the mixed-layer water that was sampled during the MR21-05C cruise. The calculations focused on the area between 72–74°N and 150–170°W (area $1.45\times10^5$ km$^2$), which included the area that we sampled in the ice margin. The volume of melted sea ice was calculated from CryoSat-2 satellite data based on the area of the sea ($1.45\times10^5$ km$^2$) and the March and October averages of ice thickness and sea-ice concentration. Our calculations indicated that the volume of sea ice declined by 260 km$^3$ over the 7 months (average 37 km$^3$ per month). The vertical profile of $\sigma_\theta$ (Figure S2c) showed that the depth of the mixed layer (the depth at which $\sigma_\theta$ was 0.125 kg m$^{-3}$) varied from 6 m to 19 m and averaged 12 m. We assumed the sea-ice density to be 910 kg m$^{-3}$ (Mahoney et al., 2015). The concentrations of nutrients in the sea ice that we used in the calculations were the averages of sea ice or high-turbidity ice collected in this study, and nutrient concentrations in seawater were the averages of the concentrations in the mixed layer (**Tables 2** and **3**).

We next calculated the primary production ($PP_{ice}$) that could be supported by the nutrients supplied by the melting of sea ice in the same area. The data used in the calculations were the same as those described above. The concentration of dissolved inorganic nitrogen (DIN = $NO_3^- + NO_2^- + NH_4^+$) in sea ice was assumed to be either 2.7 μmol L$^{-1}$, the mean value of all sea ice, or 6.5 μmol L$^{-1}$, the value for high-turbidity ice (**Table 2**). The volume of sea-ice melt was 260 km$^3$, the difference of the volume of sea ice between March (when the extent of the sea ice was at maximum) and October (when it was at minimum). Nitrogen was assumed to be the limiting nutrient in the seawater after the sea ice melted (**Table 3**). Primary production was calculated assuming a C:N ratio of 6.4 for the Chukchi Sea and Canada Basin based on Frigstad et al. (2014). We assumed that all DIN in the sea ice was assimilated.

Primary production based on the nutrient concentrations in seawater ($PP_{sea}$) was calculated for comparison. The difference between the DIN concentration of seawater obtained from water sampling and the average DIN concentration in the TML was calculated by water-column integration and conversion to carbon assuming a C:N ratio of 6.4. For simplicity, the target area was divided at 160°W. The area west of 160°W was defined as the shelf area and the area east of 160°W was defined as the basin area. The integral was calculated to the bottom for the shelf area and to the TML for the basin area. Other parameters such as the N:P ratio and period of time were the same as those used in the calculation of sea-ice-derived primary production. The data used in this calculation came from four seawater stations west of 160°W and six seawater stations east of 160°W. Data from seawater station 23, which was located on the shelf east of 160°W, were excluded from the calculations.

## 3. Results

### 3.1. Physical properties of sea ice

Sea-ice surface and interior temperatures ranged from −1.3°C to −1.0°C and −1.3°C to −0.8°C, respectively, with average values of −1.2°C ± 0.2°C (n = 8) and −1.1°C ± 0.2°C (n = 8), respectively (Table S1). The mean value of the sea-ice surface and interior temperatures taken together was −1.2°C ± 0.2°C (n = 16; **Table 2**).

Sea-ice salinity ranged from 0.0 to 2.6 (**Figure 2a**), with an average of 1.2 ± 0.8 (n = 71; **Table 2**). The salinity at station ICE1 ranged between 0.0 and approximately 1.0,

**Table 2. Temperature, salinity, concentrations of nutrients and chlorophyll-a (chl-a), turbidity, and $\delta^{18}O$ (mean ± standard deviation) for sea ice, snow, surface water (depth of 5 m), temperature minimum layer (TML), and sea ice with high turbidity (>3.2 FTU)**

| Sample Type (n value) | Temperature (°C) | Salinity | $NO_3^-$ (μmol $L^{-1}$) | $NO_2^-$ (μmol $L^{-1}$) | $Si(OH)_4$ (μmol $L^{-1}$) | $PO_4^{3-}$ (μmol $L^{-1}$) | $NH_4^+$ (μmol $L^{-1}$) | DIN[a] (μmol $L^{-1}$) | Chl-a (μg $L^{-1}$) | Turbidity (FTU) | $\delta^{18}O$ (‰) |
|---|---|---|---|---|---|---|---|---|---|---|---|
| Sea ice (71) | −1.2 ± 0.2 | 1.2 ± 0.8 | 1.0 ± 1.1 | 0.1 ± 0.1 | 0.5 ± 0.5 | 0.8 ± 3.7 | 1.6 ± 3.8 | 2.7 ± 3.9 | 1.0 ± 1.7[b] | 1.6 ± 2.3 | −2.3 ± 1.9 |
| Snow (29) | —[c] | — | — | — | — | — | — | — | — | — | −14.8 ± 6.0 |
| Surface water (11) | +0.7 ± 1.0 | 28.3 ± 1.7 | 0.1 ± 0.1 | 0.0 ± 0.0 | 3.1 ± 0.9 | 0.5 ± 0.0 | 0.1 ± 0.1 | 0.1 ± 0.2 | — | — | — |
| TML (6) | −1.6 ± 0.1 | 33.1 ± 0.1 | 15.6 ± 1.4 | 0.1 ± 0.1 | 38.7 ± 6.3 | 1.9 ± 0.2 | 0.8 ± 0.6 | 16.5 ± 1.7 | — | — | −1.4 ± 0.1[d] |
| High-turbidity ice (11) | — | 1.5 ± 0.4 | 0.6 ± 0.5 | 0.1 ± 0.1 | 1.1 ± 1.0 | 4.8 ± 8.6 | 5.8 ± 8.3 | 6.5 ± 8.4 | 4.1 ± 2.1 | 6.3 ± 2.2 | −1.5 ± 1.0 |

[a]Dissolved inorganic nitrogen (DIN = $[NO_3^-] + [NO_2^-] + [NH_4^+]$).

[b]n = 70.

[c]No data (—).

[d]n = 3.

**Table 3. Effect of sea-ice meltwater on salinity and nutrient concentrations (mean ± standard deviation, n =18) in the mixed layer**

| | | Nutrient Concentration (μmol $L^{-1}$) | | | | | |
|---|---|---|---|---|---|---|---|
| **Data Type** | **Salinity** | **$NO_3^-$** | **$NO_2^-$** | **$Si(OH)_4$** | **$PO_4^{3-}$** | **$NH_4^+$** | **DIN[a]** |
| Mixed layer (before) | 28.6 ± 1.7 | 0.1 ± 0.2 | 0.0 ± 0.0 | 3.1 ± 0.9 | 0.5 ± 0.0 | 0.1 ± 0.1 | 0.2 ± 0.3 |
| After ice melt | 25.3 | 0.2 | 0.0 | 2.8 | 0.5 | 0.3 | 0.5 |
| After high-turbidity ice melt | 25.4 | 0.1 | 0.0 | 2.9 | 1.0 | 0.8 | 0.9 |

[a]Dissolved inorganic nitrogen (DIN = $[NO_3^-]$ + $[NO_2^-]$ + $[NH_4^+]$).

which was lower than the salinity at stations ICE3 and ICE4 (**Figure 2a**). All of the salinities of sea ice collected at stations ICE3 and ICE4 exceeded 1.0 (**Figure 2a**). The salinity of the snow cover was zero (**Table 2**). Brine volume fractions of sea ice calculated from sea-ice salinity and ice temperature exceeded 5% at stations ICE3 and ICE4 and were generally below 5% at station ICE1 (**Figure 2b**, Table S2).

The $\delta^{18}O$ of sea ice ranged from −10.9‰ to −0.8‰ (**Figure 2c**) and averaged −2.3 ± 1.9‰ (n = 71; **Table 2**). The lowest value (−10.9‰) was found in the sea ice at station ICE1 (samples #13–15; **Figure 2c**). The $\delta^{18}O$ of snow cover averaged −14.8 ± 6.0‰ (n = 29; **Table 2**). The turbidity of sea ice ranged from 0.1 FTU to 9.9 FTU (**Figure 2d**) and averaged 1.6 ± 2.3 FTU (n = 71). Most of the sea-ice samples with high turbidity (e.g., station ICE1, sample #33) were brown sea ice, as shown in **Figure 3a**. The thin-section analysis showed that, for all thin-section samples, most crystals were granular in shape and the linear dimensions of most crystals were less than 1 cm (**Figure 3b–d**, **f**, **g**). Low $\delta^{18}O$ (−10.9‰) with fine-grained crystals (**Figure 3f**) characterized the snow-ice. Frazil ice was granular with similar $\delta^{18}O$ values (−2.12‰) as seawater (−1.4‰; **Figure 3b–d**, **g**).

The distribution of sea-ice ages showed that the sampling sites were located near the multiyear ice as determined by satellite imagery (white circles in **Figure 4a**).

### 3.2. Biogeochemical properties of sea ice

$NO_3^-$ concentrations of sea ice ranged from 0.0 to 6.5 μmol $L^{-1}$ (**Figure 2e**), with an average of 1.0 ± 1.1 μmol $L^{-1}$ (n = 71; **Table 2**). $NO_3^-$ concentration was higher in sea ice at station ICE4 (1.7 ± 1.5 μmol $L^{-1}$, n = 23) than at station ICE1 (0.8 ± 0.8 μmol $L^{-1}$, n = 33) and station ICE3 (0.6 ± 0.3 μmol $L^{-1}$, n = 15; Table S2, **Figure 2e**). $NO_2^-$ concentrations ranged from 0.0 to 0.5 μmol $L^{-1}$ (**Figure 2f**). The highest value (0.5 μmol $L^{-1}$) was found in sea ice at station ICE3 (**Figure 2f**). $NH_4^+$ concentration ranged from <DL to 24.4 μmol $L^{-1}$ (**Figure 2g**), with an average of 1.6 ± 3.8 μmol $L^{-1}$ (n = 71; **Table 2**). The $NH_4^+$ concentrations in sea ice varied widely (<DL–24.4 μmol $L^{-1}$) at station ICE1. The concentrations were highest in samples #30–33 at station ICE1 (**Figure 2g**). $Si(OH)_4$ concentrations in sea ice ranged from 0.1 to 3.9 μmol $L^{-1}$ (**Figure 2h**) and averaged 0.5 ± 0.5 μmol $L^{-1}$ (n = 71; **Table 2**). $PO_4^{3-}$ concentrations in sea ice ranged from <DL to 27.8 μmol $L^{-1}$ and were particularly high in samples #30–33, where they were 3.6–27.8 μmol $L^{-1}$ (**Figure 2i**). The $PO_4^{3-}$ concentrations in other samples fell in the range <DL–0.4 μmol $L^{-1}$.

The chl-a concentration was high in part of the sea ice at station ICE1 (samples #30–33), with a range of 3.6–7.1 μg $L^{-1}$, and in most of the ice at station ICE3, with a range of 0.5–5.5 μg $L^{-1}$ (**Figure 2j**). The chl-a concentrations in sea ice at station ICE4 and other samples at station ICE1 were lower, <DL–0.5 μg $L^{-1}$. The overall mean chl-a concentration in sea ice was 1.0 ± 1.7 μg $L^{-1}$ (n = 70; **Table 2**). *Nitzschia* spp. were the most dominant ice algae in the sea ice, especially in clear ice (except for samples #30–48). A comparison of the community between high-turbidity ice at stations ICE1 (samples #30–33) and ICE3 (samples #34–48) revealed that *Chaetoceros* spp. and *Cylindrotheca closterium* were dominant in high-turbidity ice at station ICE1, but *Nitzschia* spp. and *Fragilariopsis* spp. were the most abundant taxa at station ICE3.

### 3.3. Seawater properties

Surface water (5 m depth) temperatures averaged 0.7°C ± 1.0°C (n = 11; **Table 2**). Salinity ranged from 26.2 to 30.8 and averaged 28.3 ± 1.7 (n = 11). The $NO_3^-$ concentrations were <DL to 0.4 μmol $L^{-1}$ and averaged 0.1 ± 0.1 μmol $L^{-1}$ (n = 11). Most of the $NO_2^-$ concentrations were lower than the DL. The $Si(OH)_4$ concentration was 1.7–4.0 μmol $L^{-1}$, averaging 3.1 ± 0.9 μmol $L^{-1}$ (n = 11). The $NH_4^+$ concentration ranged from <DL to 0.2 μmol $L^{-1}$ and averaged 0.1 ± 0.1 μmol $L^{-1}$ (n = 11; **Table 2**).

The TML was identified at seawater stations 9, 10, 11, 15, 17, 19, and 22 (**Table 1**, Figure S2a). At the other seawater stations, there was no clear TML. Data from stations where the TML was clearly identified were therefore used as the TML data in this study (with $\delta^{18}O$ measured only at station 11, 17, and 19). The depth of the TML ranged from 100 m to 200 m (Figure S2a). The water temperature at the TML at those stations averaged −1.6 ± 0.1°C (n = 6) and did not differ significantly among those stations (**Table 2**). The salinity at the TML at each station ranged from 32.9 to 33.1 (Figure S2b) and averaged 33.1 ± 0.1 (n = 6; **Table 2**). The $NO_3^-$ concentration range was 14.4–18.4 μmol $L^{-1}$, averaging 15.6 ± 1.4 μmol $L^{-1}$ (n = 6). The $NO_2^-$ concentration was <DL to 0.2 μmol $L^{-1}$, averaging 0.1 ± 0.1 μmol $L^{-1}$ (n = 6); that of $PO_4^{3-}$ was 1.8–2.3 μmol $L^{-1}$, averaging 1.9 ± 0.2 μmol $L^{-1}$ (n = 6); and that of $NH_4^+$ was <DL to 1.5 μmol $L^{-1}$, averaging 0.8 ± 0.6 μmol $L^{-1}$ (n = 6; **Table 2**). The $\delta^{18}O$ at TML (seawater stations 11, 14, and 17) ranged

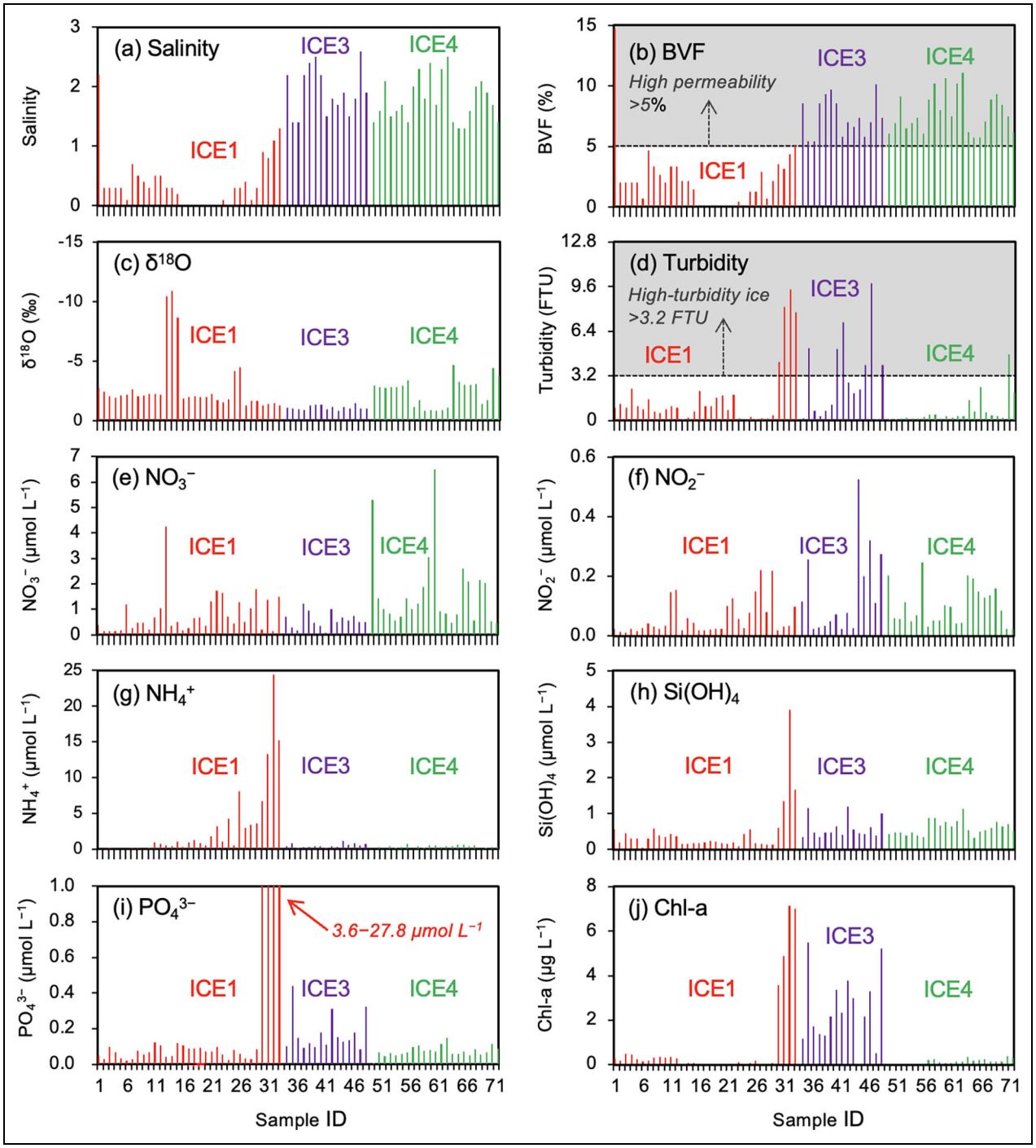


**Figure 2. Characteristics of the brash ice samples.** Bar graphs of (a) salinity, (b) brine volume fraction (BVF), (c) $\delta^{18}O$, (d) turbidity, and concentrations of (e) $NO_3^-$, (f) $NO_2^-$, (g) $NH_4^+$, (h) $Si(OH)_4$, (i) $PO_4^{3-}$, and (j) chlorophyll-a (chl-a) for each brash ice sample from stations ICE1, ICE3, and ICE4 (**Figure 1**). The gray-shaded areas indicate (b) high permeability ice (>5% BVF) and (d) high turbidity ice (>3.2 FTU).

from −1.4‰ to −1.3‰ (mean of −1.4 ± 0.1‰, n = 3; **Table 2**).

The vertical profile of potential density $\sigma_\theta$ (Figure S2c) showed that the depth of the mixed layer (the depth at which $\sigma_\theta$ was 0.125 kg $m^{-3}$) ranged from 6 m to 19 m and averaged 12 m. The depth of the mixed layer was deepest (19 m) at the westernmost station, seawater station 30, and shallowest (6 m) at seawater station 19 in the Canadian Basin (Figure S2c).

### *3.4. Estimation of impact of sea-ice melt*

The results of the calculations for the potential of sea-ice meltwater to alter nutrient concentrations are provided in **Table 3**. When sea ice melted, the salinity and the concentration of $Si(OH)_4$ were decreased (diluted), whereas the concentrations of $NO_3^-$ and $NH_4^+$ increased. The concentrations of $NO_2^-$ and $PO_4^{3-}$ remained almost unchanged. When the high-turbidity ice melted, the results were qualitatively similar to the results based on

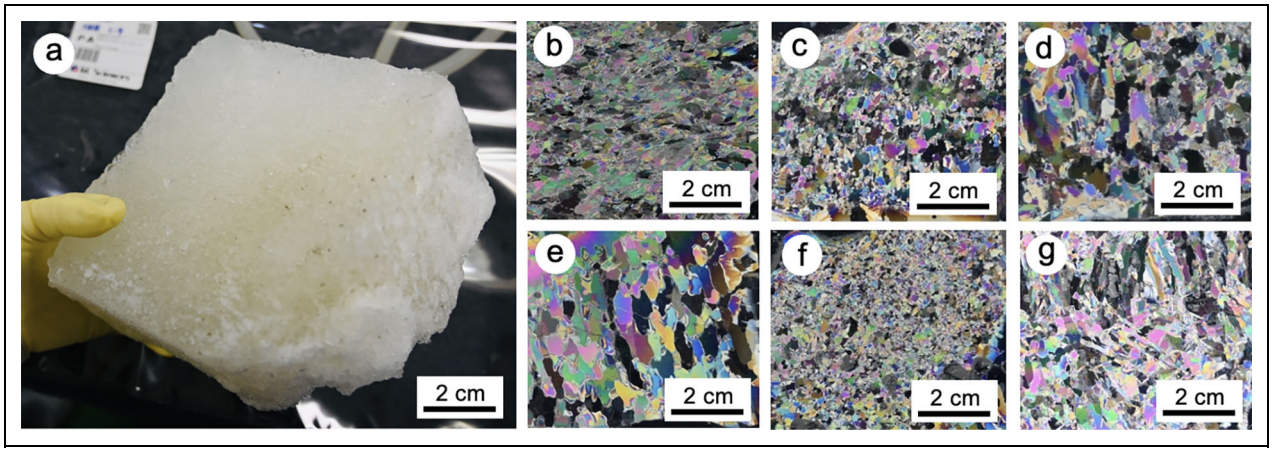


**Figure 3. Images of brown ice and thin-sectioned brash ice from station ICE1.** Images of (a) brown sea ice (sample #33) and thin sections of brash sea ice for (b) top section (sample #1), (c) middle section (sample #2), (d) bottom section (sample #3), (e) columnar ice (sample #24), (f) low-$\delta^{18}O$ ice (sample #14), and (g) high-turbidity ice (sample #31). Images b–g were obtained under crossed polarizers.

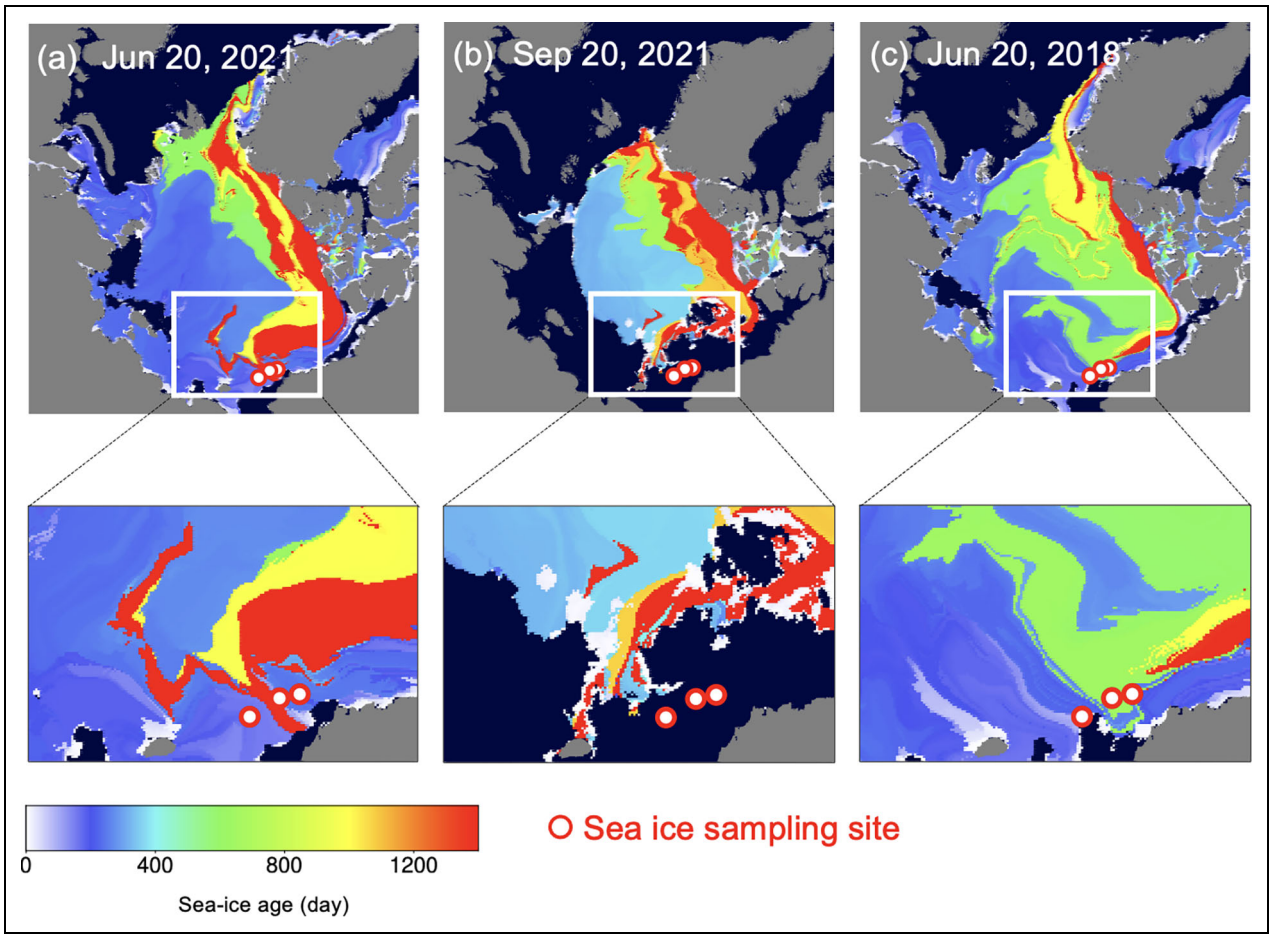


**Figure 4. Distribution of sea ice age.** Distribution of sea-ice ages in the Arctic Ocean for (a) June 20, 2021, (b) September 20, 2021, and (c) June 20, 2018, with corresponding enlargements of the study area. These images were produced from AMSR-2 satellite data (Kimura et al., 2022).

the mean value of all sea ice. However, the amount of change was larger for concentrations of $PO_4^{3-}$ and $NH_4^+$, and the degree of dilution of the $Si(OH)_4$ concentration was smaller. The concentrations of $NO_3^-$ and $NO_2^-$ changed very little from their concentrations in the mixed layer before melting (**Table 3**).

The primary production ($PP_{ice}$) that could be supported by the nutrients supplied by the melting of sea ice in the same area is shown below. When the calculations were based on the average of all sea ice ($PP_{ice\text{-}mean}$), the DIN was supplied at $2.0 \times 10^{-2}$ µmol $m^{-2}$ $d^{-1}$ for 7 months from March to October, and the average $PP_{ice\text{-}mean}$ was

1.6 mg C $m^{-2}$ $d^{-1}$. When the calculations were based on the average for high-turbidity ice ($PP_{ice\text{-}high\ turbidity}$), DIN was supplied at 4.8 $\times$ $10^{-2}$ μmol $m^{-2}$ $d^{-1}$, and the $PP_{ice\text{-}high\ turbidity}$ was 3.7 mg C $m^{-2}$ $d^{-1}$. The primary production based on the nutrient concentrations in ocean water ($PP_{sea}$) averaged 140 $\pm$ 40 mg C $m^{-2}$ $d^{-1}$ (n = 4) over the shelf area and 460 $\pm$ 100 mg C $m^{-2}$ $d^{-1}$ (n = 6) over the basin area, with an average for the whole area of 300 mg C $m^{-2}$ $d^{-1}$.

## 4. Discussion

In this section, we will discuss: (1) age of the sea ice sampled in this study based on analysis of satellite data; (2) potential drivers of nutrient distribution in brash sea ice compared with those of winter seawater, from which sea ice is formed, and first-year ice core data; (3) characteristics of the dirty ice with high chl-a concentration and turbidity; and (4) the effect of sea-ice melting on nutrient concentrations in the surface layer of this region of the Arctic Ocean.

### *4.1. Age of sea ice sampled in this study*

According to satellite data in June 2021, the sampling sites were near the regions of multiyear ice (white circles in **Figure 4a**). The sea ice sampled in this study was therefore considered likely to have been multiyear ice (4–5 years old; **Figure 4a**). Furthermore, an examination of the distribution of the ages of sea ice during the month of sampling (September 2021; **Figure 4b**) revealed that multiyear ice remained in the vicinity of the ice sampling sites.

In contrast, comparison of sea-ice age distribution in June 2021 with that in June 2018 (**Figure 4c**) revealed that the oldest of the multiyear ice (red) was particularly widely distributed in 2021 from the Beaufort Sea to the Chukchi Sea. Because most of the sea ice in the Beaufort and Chukchi seas melts in the summer, more multiyear ice may have melted in the northern Chukchi Sea and Canada Basin in 2021.

### *4.2. Potential drivers of nutrient distribution in sea ice*

The chl-a concentrations in the brash ice in this study (range of 3.6–7.1 μg $L^{-1}$, mean of 1.0 μg $L^{-1}$; **Table 2**) feel within the range of observed chl-a concentrations in multiyear ice in Fram Strait (0.1–12.1 μg $L^{-1}$, mean of 1.0 μg $L^{-1}$; Meiners et al., 2003). The high chl-a concentrations observed in part of the brash ice at stations ICE1 (samples #30–33) and ICE3 suggest high concentrations of organic matter (algal biomass) in the ice.

To assess the impact of nutrient consumption and organic-matter decomposition within sea ice on various nutrient concentrations within the ice, we examined the relationship between nutrient concentrations and salinity. In the absence of any biological activity or allochthonous nutrient supply, the salinity and nutrients in sea ice decrease at the same rate because of brine discharge. A plot of nutrient concentration versus salinity in sea ice is therefore a straight line (dilution line) that connects the salinity and nutrient concentration of seawater at the time of formation (Thomas et al., 1995). However, in collected sea ice, the plot deviates from the dilution line because of biological activity and allochthonous inputs of nutrients.

In this study, dilution lines were drawn based on the salinity and nutrient concentrations of the Arctic Ocean surface water and TML sampled during MR21-05C. We examined the deviation of the plots from the dilution lines. Seawater in the TML reflects winter conditions (Pondaven et al., 2000; Tomczak and Liefrink, 2005). A deviation above that dilution line (hereafter referred to as the TML dilution line) indicates organic matter remineralization, dissolution of diatom frustules, or allochthonous sources (e.g., Thomas et al., 1995), and a deviation below indicates consumption of nutrients by ice algae. Furthermore, a comparison of the surface-water dilution line with the nutrient concentrations of sea ice enables an assessment of the impact of sea-ice melting on surface water during the summer months (details are given in Section 4.4).

The concentrations of all nutrients in surface water in this study were low (**Table 2**), and all nutrient concentrations were above the surface-water dilution line (**Figure 5a**–**f**). The BVFs exceeded 5% for sea ice at stations ICE3 and ICE4 and were generally below 5% for sea ice at station ICE1 (**Figure 2b**). When the BVF exceeds 5%–7.5%, brine flows and seawater exchange occurs (Golden et al., 1998; Pringle et al., 2009; Zhou et al., 2013). The sea ice at station ICE1 was thus not considered affected by the low-nutrient seawater because BVF was below 5% and exchange with low-nutrient seawater would have been negligible. The sea ice at stations ICE3 and ICE4, however, was highly permeable and would be affected by low-nutrient seawater.

The range of $NO_3^-$ concentrations given by Deming et al. (2020) for first-year landfast ice (hereafter referred to as first-year ice) is 0.2–10.2 μmol $L^{-1}$, which is roughly the same as the range of $NO_3^-$ concentrations in the brash ice obtained in this study (<DL–6.5 μmol $L^{-1}$; **Figure 2e**). The $NO_3^-$ values of this brash ice generally fell above the TML dilution line (**Figure 5a**); in particular, sea ice at station ICE1 tended to plot above the TML dilution line, whereas most of the sea-ice data at station ICE3 fell below that line (**Figure 5a**).

When nitrogen-containing organic matter decomposes, ammonium is regenerated first, and then the ammonium is converted to $NO_2^-$ and $NO_3^-$ by nitrification (e.g., Thomas et al., 2010). In the Arctic, $NO_3^-$ is also supplied to sea ice by snowfall (Granskog et al., 2003; Krell et al., 2003). The fact that graphs of nitrate versus salinity at stations ICE1 and ICE4 were above the TML dilution line implies that there was an allochthonous supply of nitrate from snowfall or seawater or that the supply via nitrification exceeded the consumption by assimilation. In contrast, the fact that the data at station ICE3 fell below the TML dilution line implies that the supply via nitrification was less than the consumption via assimilation. Because nitrification is affected by light, pH, and the concentration of ammonium (Guerrero and Jones, 1996a, 1996b; Martens-Habbena et al., 2009; Beman et al., 2010; Kitidis et al., 2011; Merbt et al., 2012; Horak et al., 2013; Qin

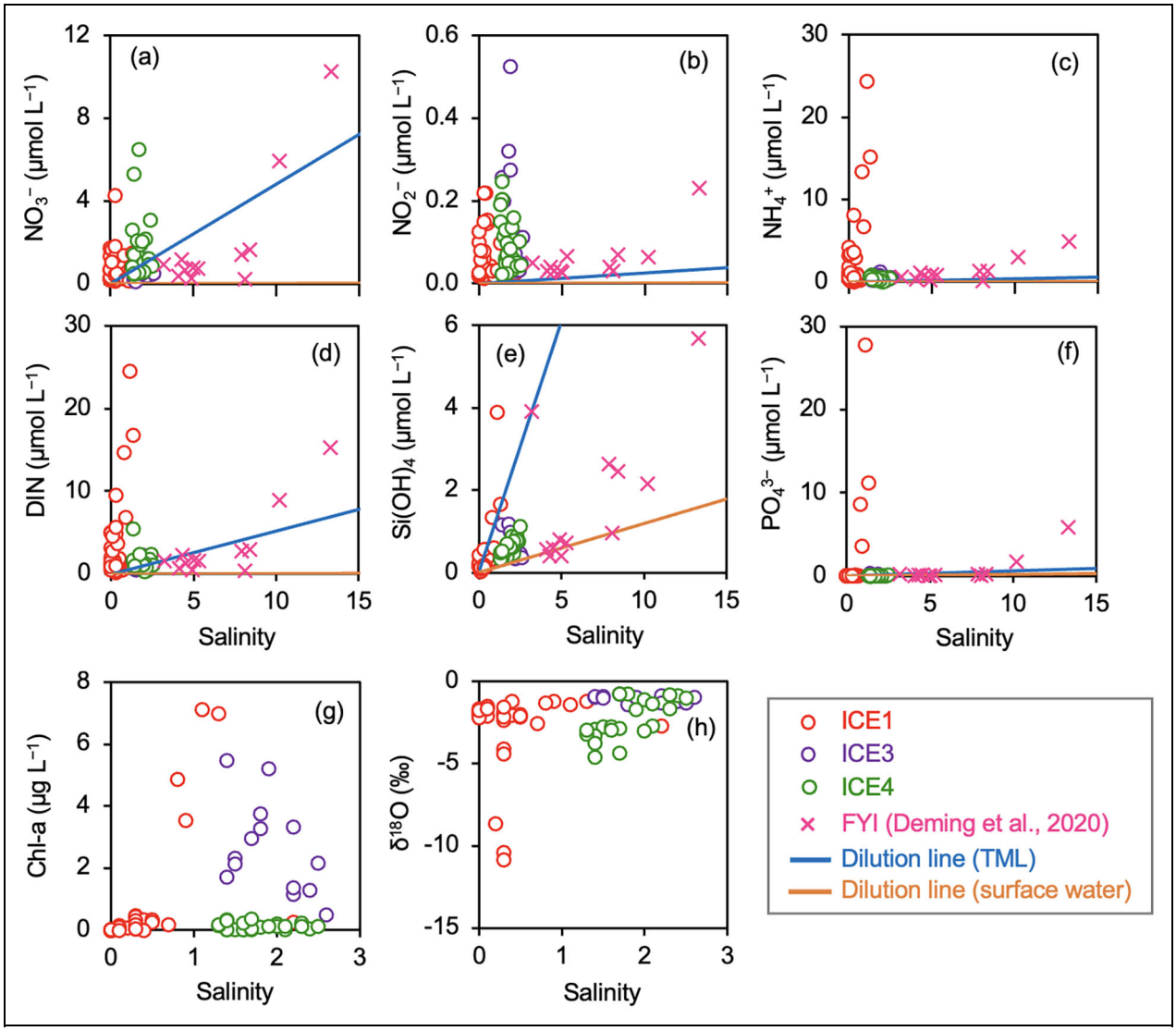


**Figure 5. Plots of nutrient concentrations, chlorophyll-a concentration, and $\delta^{18}O$ versus salinity.** Plots of nutrient concentrations, chlorophyll-a (chl-a) concentration, and $\delta^{18}O$ versus salinity for brash ice at stations ICE1, ICE3, and ICE4 and (a–f) first-year ice (FYI) cores from Deming et al. (2020) for (a) $NO_3^-$, (b) $NO_2^-$, (c) $NH_4^+$, (d) dissolved inorganic nitrogen (DIN = $[NO_3^-] + [NO_2^-] + [NH_4^+]$), (e) $Si(OH)_4$, (f) $PO_4^{3-}$, (g) chl-a, and (h) $\delta^{18}O$. Dilution lines were obtained based on the nutrient concentrations and salinity of the temperature minimum layer (TML) and surface water.

et al., 2014), the combined effect of all of these factors must be considered.

$NO_2^-$ and $NH_4^+$ were both virtually absent in the TML and surface water (**Table 2**), yet the concentrations of both in the brash ice were above the TML dilution line (**Figure 5b**, **c**). Because surface seawater contained little $NH_4^+$ (**Table 2**), a supply via seawater seepage is unlikely. Regeneration of $NH_4^+$ by decomposition of organic matter is therefore likely the source of the $NH_4^+$ that would be subsequently assimilated and oxidized (nitrification; Fripiat et al., 2017). The concentrations of $NH_4^+$ in some samples at station ICE1 (samples #31–33) were very high, 10.0–24.4 µmol L$^{-1}$ (**Figure 2g**). By comparison, Deming et al. (2020) reported that the range of $NH_4^+$ concentrations in first-year ice was 0.2–4.9 µmol L$^{-1}$, with the highest values at the top (1.3 µmol L$^{-1}$) and bottom (3.0–4.9 µmol L$^{-1}$) of the ice. In addition, Tovar-Sánchez et al. (2010) reported that the range of $NH_4^+$ concentrations in multiyear ice along the Greenland Current and Fram Strait in July was 0.7–1.4 µmol L$^{-1}$. The relatively high chl-a concentration in the sea ice at station ICE3 (**Figure 2j**, Table S2) suggests that a large amount of nitrogen was fixed in biomass. To explain the high concentrations of both $NH_4^+$ and biomass at station ICE3, we suggest that DIN was likely being supplied from allochthonous sources.

The concentrations of $Si(OH)_4$ were below the TML dilution line (**Figure 5e**). $Si(OH)_4$ is consumed by diatoms to make their silica frustules and is regenerated by the dissolution of the frustules after diatom death (Fripiat et al., 2017). On the other hand, high concentrations of $Si(OH)_4$ in some samples (station ICE1) with respect to the TML dilution line likely reflected the dissolution of diatom silica frustules over a long period of time. The concentrations of $Si(OH)_4$ in this study were higher than those in

multiyear ice (0.01–0.26 μmol $L^{-1}$) reported by Tovar-Sánchez et al. (2010).

The concentrations of $PO_4^{3-}$ were above the TML dilution line (**Figure 5f**), indicating that remineralization of $PO_4^{3-}$ had progressed. The concentrations of $PO_4^{3-}$ in some sea ice at station ICE1 (samples #30–33) were much higher (3.6–27.8 μmol $L^{-1}$) than observed in previous studies (<0.2 μmol $L^{-1}$; Meiners et al., 2003; <1.0 μmol $L^{-1}$, Werner et al., 2007; <0.17 μmol $L^{-1}$, Tovar-Sánchez et al., 2010).

The first-year ice collected by Deming et al. (2020) was younger than the samples of the MR21-05C cruise in this study and had a higher salinity (3.2–13.3 versus 0.0–2.6; **Figure 2a**). Compared to first-year ice, the samples of MR21-05C tended to plot above the TML dilution line for $NO_3^-$, $NO_2^-$, $NH_4^+$, and $PO_4^{3-}$ and therefore reflected nutrient remineralization over time. $Si(OH)_4$ concentrations were below the TML dilution line and therefore reflected the slow remineralization of $Si(OH)_4$, as described above. With the exception of $Si(OH)_4$, the nutrient concentrations in the MR21-05C sample were higher than expected from its low salinity relative to first-year ice (**Figure 5a**–**f**).

In the ocean, turbidity depends on the concentrations of sediment (mineral particles) and phytoplankton (Giesen et al., 1990). Similarly, samples of sea ice with highly turbid meltwater are considered to contain numerous aeolian mineral particles, suspended solids that were incorporated into the sea ice during the period of ice formation, and ice algae (Eicken et al., 2000; Eicken et al., 2005; Waga et al., 2022). Here $\delta^{18}O$ values are used to help explain the source of particles in the sampled brash ice, as $\delta^{18}O$ is lower for meteoric waters such as snow and rain (e.g., Jeffries et al., 1994) relative to the seawater value of nearly zero. Therefore, the $\delta^{18}O$ of the brash ice obtained in this study, which averaged −2.31‰ (**Table 2**), was derived mainly from seawater. However, we considered the sea ice at station ICE1 (samples #13–15; −8.6‰ to −10.9‰), where the $\delta^{18}O$ was particularly low, to be derived mostly from snow. When we compared the $\delta^{18}O$ and turbidity results, we found a trend of low turbidity in sea ice with low $\delta^{18}O$ and high turbidity in sea ice with high $\delta^{18}O$ (**Figure 2c**, **d**). This trend suggests that sediments in the seawater and ice algae growing in the sea ice most likely affected the turbidity, whereas suspended particles such as mineral particles from atmospheric deposition had little effect. In the thin-section photographs shown in **Figure 3b**–**g**, the crystals were finer at the top of the sea ice (**Figure 3b**) and slightly larger at the bottom (**Figure 3d**). The $\delta^{18}O$ was −2.8‰ at the top, −2.4‰ at the middle, and −2.0‰ at the bottom. The fact that the $\delta^{18}O$ was lowest at the top suggests a marked influence of upper snow on the formation of snow-ice. The fact that the crystal sizes of the sea ice with particularly low $\delta^{18}O$ (−10.9‰) were finer (**Figure 3f**) is consistent with an origin mostly from snow. In contrast, the fact that crystals of ice with high concentrations of $PO_4^{3-}$ and $NH_4^+$ (sample #31; **Figure 2g**, **i**) were slightly larger than the fine-grained crystals of snow-ice (Sahashi et al., 2022) suggests that they originated from seawater.

### 4.3. Characteristics of dirty ice

The sea ice at station ICE1 (samples #30–33) had higher concentrations of $PO_4^{3-}$ and $NH_4^+$ (3.6–27.8 μmol $L^{-1}$ and 6.7–24.4 μmol $L^{-1}$, respectively) than the other samples (0–0.4 μmol $PO_4^{3-}$ $L^{-1}$ and 0–8.1 μmol $NH_4^+$ $L^{-1}$; **Figure 2g**, **i**) as well as higher concentrations of chl-a (3.6–7.1 μg $L^{-1}$) than the other samples (0–5.5 μg $L^{-1}$; **Figure 2j**). The color of this ice was brown (**Figure 3a**). The high concentrations of organic matter (algal biomass) and eutrophic nature of such "dirty ice" need to be evaluated, because they are likely to have a marked impact on the surrounding seawater environment when the ice melts. In this section, we focus on dirty ice and the biogeochemical processes that occur in dirty ice.

Dirty ice is ubiquitous in the Arctic Ocean (Eicken et al., 2000; Eicken et al., 2005; Waga et al., 2022). The formation of dirty ice is mainly due to entrainment of sediments resuspended from the seafloor into the sea ice (e.g., Eicken et al., 2000). Waga et al. (2022) estimated the distribution and seasonal changes of dirty ice in the Arctic Ocean based on differences in albedo obtained from satellite observations, reporting that dirty ice accounts for 50% of sea ice in late summer in the Canada Basin. In this study, we used the turbidity of sea-ice meltwater to assess quantitatively the particle load of the sea ice. **Figure 6** shows the relationships between turbidity and the concentrations of various nutrients and chl-a in the ice. There was little correlation between turbidity and the concentrations of $NO_3^-$ and $NO_2^-$ ($r^2 < 0.03$, $p > 0.07$; **Figure 6a**, **b**); in contrast, the concentrations of $NH_4^+$, $Si(OH)_4$, and $PO_4^{3-}$ increased with increasing turbidity (**Figure 6c**–**e**). The correlation was highest between turbidity and the chl-a concentration in sea ice ($r^2 = 0.67$, $p < 0.001$; **Figure 6f**). In the following discussion, we focus on samples with high turbidity and chl-a concentrations, and on the relationship between turbidity and biological processes. Here, we define high-turbidity sea ice to be sea ice with a turbidity greater than twice our sea-ice sample mean of 1.6 FTU (**Table 2**); that is, >3.2 FTU.

The chl-a concentrations at station ICE3 were relatively high (**Figure 2j**) in high-turbidity ice (**Figure 2d**). The concentrations of nutrients, however, were almost the same in high-turbidity ice and ice with lower turbidities (**Figure 2e**–**i**). Examination of salinity versus nutrient relationships for station ICE3 revealed that the concentrations of $NO_3^-$ and $Si(OH)_4$ were below the TML dilution line, whereas the concentrations of $NO_2^-$, $NH_4^+$, and $PO_4^{3-}$ were above the TML dilution line (**Figure 5**). The fact that the DIN concentrations were on the TML dilution line (**Figure 5d**) indicates that the concentrations of DIN could be explained by brine discharge, assimilation by ice algae, and decomposition of organic matter. In contrast, the high-turbidity ice at station ICE1 was characterized by high concentrations of chl-a, $NH_4^+$, and $PO_4^{3-}$ (**Figure 2g**, **i**, **j**). The difference between the sea ice at stations ICE1 and ICE3 was likely attributable to the difference in salinity (Table S2), which meant that the BVF

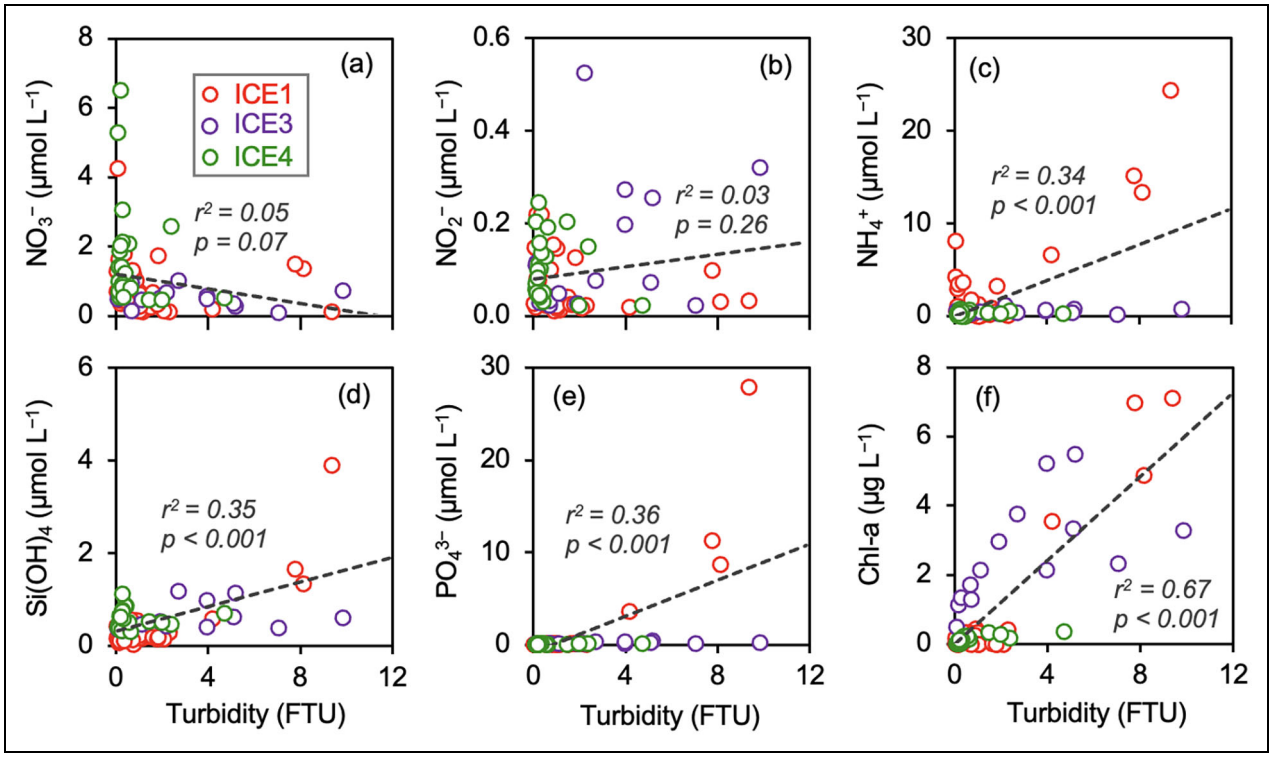


**Figure 6. Plots of nutrient and chlorophyll-a concentrations versus turbidity for brash ice.** These figures show concentrations of (a) $NO_3^-$, (b) $NO_2^-$, (c) $NH_4^+$, (d) $Si(OH)_4$, (e) $PO_4^{3-}$, and (f) chlorophyll-a (chl-a) for brash ice from stations ICE1, ICE3, and ICE4. Gray dashed lines indicate regression lines.

exceeded 5% at station ICE3 and was generally less than 5% at station ICE1. The implication is that station ICE3 may have been infiltrated by surface water with low nutrient concentrations, and the nutrient concentrations in the sea ice were therefore low. In addition, the composition of the ice algae at station ICE1 differed from that of the high-turbidity ice at station ICE3. The main algal species were *Chaetoceros* spp. and *Cylindrotheca closterium* at station ICE1 and *Nitzschia* spp. at station ICE3. Differences in nutrient consumption trends and the characteristics of EPS secretion due to differences in constituent species may have caused the difference in the trends between stations ICE1 and ICE3. The high-turbidity ice also contained significantly higher concentrations of $NH_4^+$, $PO_4^{3-}$, and chl-a (**Figure 2g**, **i**, **j**). The concentrations of $Si(OH)_4$ were also higher in the high-turbidity ice (**Figure 2h**), although the difference was less apparent. Because phytoplankton grow by consuming nutrients in the sea ice, understanding why the concentrations of chl-a and nutrients were simultaneously high is difficult. However, Roukaerts et al. (2021) have reported that a sea ice-nutrient paradox can occur in which an increase in ice algal biomass and nutrient accumulation occurs simultaneously within sea ice. This sea ice-nutrient paradox occurred in the high-turbidity ice in this study. The N:P ratios (DIN:$PO_4^{3-}$) were 0.9–1.9 in the high-turbidity ice at station ICE1. These ratios are much lower than the Redfield ratio of 16. The N:P ratio of the high-turbidity ice at station ICE3 was 3.1–10.4, that is, lower than the Redfield ratio and the ratio associated with diatom uptake. The reasons for such low N:P ratios (excess of P relative to N) are discussed below.

According to Fripiat et al. (2017), the excess (accumulation) of $PO_4^{3-}$ relative to DIN can be explained by (1) rapid remineralization of P relative to N, (2) denitrification, (3) decomposition of P-rich organic matter, and (4) adsorption of $PO_4^{3-}$ onto sea ice. With the lack of oxygen data, however, denitrification cannot be confirmed. Adsorption to EPS and retention within the biofilm is potentially the main pathway for $PO_4^{3-}$ accumulation in Arctic brash ice, as previously suggested in Antarctic sea ice (Roukaerts et al. 2021).

We next discuss the reasons for the accumulation of $NH_4^+$. The BVF of the high-turbidity ice was generally less than 5% (**Figure 2b**). This information, combined with the fact that the $NH_4^+$ concentration was lower in surface water (0.1 µmol L$^{-1}$) than in sea ice, suggests that seawater intrusion was unlikely to have been the source of the $NH_4^+$. An alternative explanation is that the organic matter accumulated during spring and summer and then began to decompose during the fall as growing conditions deteriorated. The decomposition then resulted in the formation of $NH_4^+$. $NH_4^+$ is known to be adsorbed by the EPS secreted by ice algae (Fripiat et al., 2017), and such adsorption may have contributed to the accumulation of $NH_4^+$. Frantz et al. (2019) reported the heavily melted porous (rotten) first-year ice at offshore near Barrow (Utqiaġvik), Alaska, in July 2015 and 2017 for physical and optical characteristics of sea ice. Because rotten ice is extremely porous (>10%) and pore spaces within ice are

typically well connected to the ocean, organic matter and sediment within sea ice are flushed out. Therefore, nutrients dynamics within rotten ice may differ from those observed in our high-turbidity brash ice.

Snowfall is known to be a source of $NO_3^-$ and $NH_4^+$ (Kaartokallio, 2001; Granskog et al., 2003; Krell et al., 2003; Nomura et al., 2010; Nomura et al., 2011). The snow fraction for high-turbidity ice ranged from 17.0% to 18.2%. These values were within the range of snow fractions reported for Saroma-ko Lagoon along the Sea of Okhotsk (1%–47%; Nomura et al., 2011) and the Southern Ocean (2%–52%; Nomura et al., 2023b). In this study, there was no apparent correlation between $NO_3^-$ or $NH_4^+$ and the snow fraction (Figure S3). Hence, factors other than snow were significant sources of DIN.

Roukaerts et al. (2021) reported that $NO_3^-$ increases as ice algal biomass increases, but the accumulation of $NO_3^-$ was not as pronounced as the accumulation of $NH_4^+$ and $PO_4^{3-}$ in the high-turbidity ice in this study. Regeneration of $NH_4^+$ may have occurred because of the decomposition of organic matter, but nitrification did not progress, perhaps because nitrification is inhibited by a high-light environment (Guerrero and Jones, 1996a, 1996b; Horak et al., 2018; Shiozaki et al., 2019).

### *4.4. Assessing the impact of melting sea ice on the nutrient environment of surface seawater*

We estimated the impact of melting sea ice on the nutrient environment of the sea surface based on our observations. We first considered the impact of sea-ice meltwater on the summer surface water based on the deviation of nutrient concentrations from the surface-water dilution line, which was drawn based on the salinity and nutrient concentrations in the summer surface water. If the sea-ice data were above the surface-water dilution line, the indication would be that the sea-ice meltwater provided nutrients to the surface water. Most of the sea-ice nutrient concentrations were above the surface-water dilution line for all nutrients (**Figure 5**). The surface water of the northern Chukchi Sea and Canada Basin is almost completely depleted of nutrients during the summer months (**Table 2**), and the melting of sea ice could provide a source of nutrients.

Next, we considered the potential of sea-ice melt to alter nutrient concentrations. We first examined the results of the calculations based on the average of all sea ice (**Table 3**). After melting of sea ice, the salinity and the concentration of $Si(OH)_4$ were decreased (diluted), whereas the concentrations of $NO_3^-$ and $NH_4^+$ increased. Therefore, melting sea ice may provide $NO_3^-$ to $NO_3^-$-depleted seawater (Nishino et al., 2016) to support phytoplankton growth. Although melting of sea ice decreased the concentration of $Si(OH)_4$, it was present in sufficient amounts relative to $NO_3^-$ that diatom growth was unlikely to have been limited by silicate. When the high-turbidity ice melted, the concentrations of both $PO_4^{3-}$ and DIN were about twice the concentrations estimated based on the mean value of all sea ice (**Table 3**). The implication is that the impact of the melting of high-turbidity ice on the supply of nutrients, especially $PO_4^{3-}$ and DIN, was pronounced. Based on these calculations, we conclude that the melting of high-turbidity ice has a notable impact

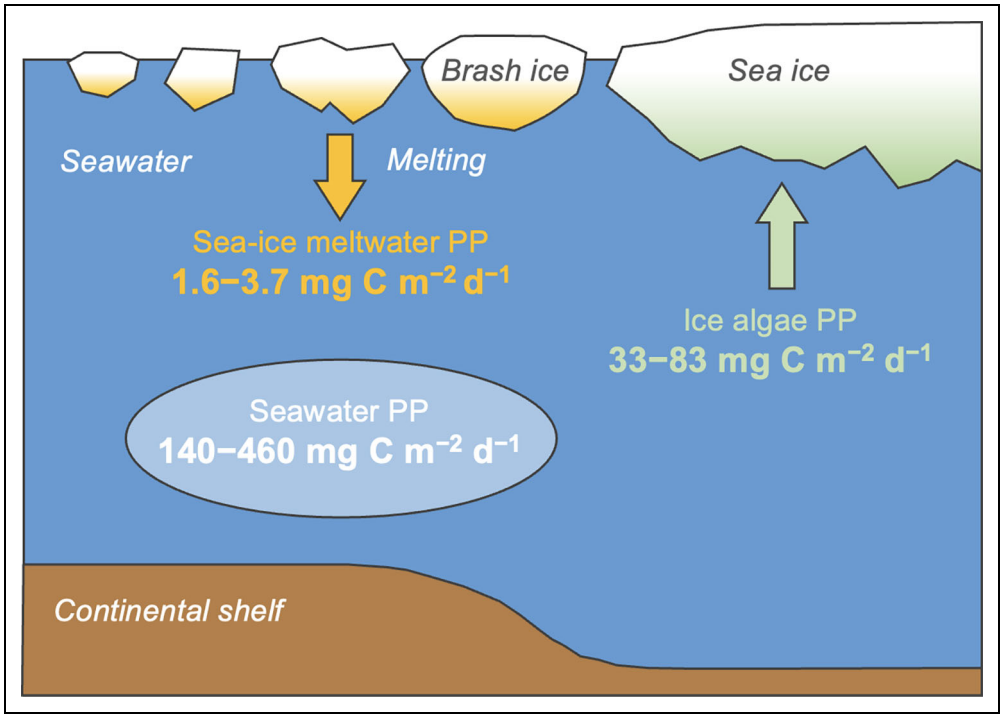


**Figure 7. Schematic illustration of primary production.** Primary production (PP) was estimated based on the nutrient concentrations within sea ice (Sea-ice meltwater PP) and seawater in the Chukchi Sea (Seawater PP). Primary production by ice algae (Ice algae PP) was obtained from Subba Rao and Platt (1984), Legendre et al. (1992), and Gosselin et al. (1997).

on the nutrient concentrations in the marine environment. While we fixed the depth of the MLD in our calculations, sea ice actually melts gradually. The results presented here thus reflect the maximum impact of sea-ice meltwaters on nutrient reservoirs. As the Arctic region is currently experiencing rapid sea-ice melt, our calculations are relevant to the predicted changes in surface stratification and associated nutrient stocks and primary productivity.

We next calculated the primary production ($PP_{ice}$) that could be supported by the nutrients supplied by the melting of sea ice in the same area. The $PP_{ice\text{-}mean}$ was 1.6 mg C $m^{-2}$ $d^{-1}$ and the $PP_{ice\text{-}high\ turbidity}$ was 3.7 mg C $m^{-2}$ $d^{-1}$. When high-turbidity ice melted and the nitrogen in that meltwater was supplied to the ocean to support primary production, the impact on primary production was more than twice the impact of the average nitrogen concentration in sea-ice meltwater (**Figure 7**). Primary production based on the nutrient concentrations in ocean water ($PP_{sea}$) was calculated for comparison. This result was consistent with the primary production of 300 mg C $m^{-2}$ $d^{-1}$ in the Chukchi Sea calculated by Yun et al. (2014). Comparison of these $PP_{sea}$ and $PP_{ice}$ results shows that the $PP_{ice}$ corresponded to 0.3%–2.6% of $PP_{sea}$. The estimated primary production of 33–83 mg C $m^{-2}$ $d^{-1}$ by ice algae (Subba Rao and Platt, 1984; Legendre et al., 1992; Gosselin et al., 1997) corresponds to 1.9%–11.2% of the total production associated with sea ice.

By supplying freshwater, the melting of sea ice is usually assumed to dilute the concentrations of nutrients in the ocean surface layer and thus lower primary production (e.g., Tovar-Sánchez et al., 2010; Kanna et al., 2014). This study has shown, however, that sea-ice melting can supply nutrients, especially DIN, and support primary production in the summer Chukchi sea. Some sea ice contains more nutrients, such as the high-turbidity ice in this study and especially multiyear ice (further effected by snow). The contribution of nutrients derived from sea ice to primary production may increase as multiyear ice continues to melt with the progression of global warming until multiyear ice no longer exists in the Arctic Ocean.

## 5. Conclusions

In this study, we collected brash ice in the northern Chukchi Sea and the Canadian Basin in late summer and examined its biogeochemical composition. Nutrient concentrations other than $Si(OH)_4$ were high with respect to that of seawater. The implication is that advanced remineralization had occurred, and that the $Si(OH)_4$ concentration was low because of the slow dissolution of silica and seawater infusion with low concentrations of $Si(OH)_4$. In addition, the presence of dirty ice in the samples and the high turbidity of the meltwater reflected the presence of biological particles such as ice algae. The fact that some of the high-turbidity ice contained high concentrations of $NH_4^+$ and $PO_4^{3-}$ may have been due to adsorption on EPS secreted by ice algae. We also estimated the possible effects of sea-ice meltwater on the surface layer of the northern Chukchi Sea and Canadian Basin in summer. Sea-ice meltwater diluted the concentration of silicate, but it also supplied $NO_3^-$ and other DIN, and high-turbidity ice supplied large amounts of $NH_4^+$ and $PO_4^{3-}$. The amount of primary production supported by the DIN supplied by sea-ice meltwater was 1.6 mg C $m^{-2}$ $d^{-1}$, or 3.7 mg C $m^{-2}$ $d^{-1}$ when calculated for high-turbidity ice. We estimated this amount of primary production to correspond to 0.3%–2.6% of the primary production of 140–460 mg C $m^{-2}$ $d^{-1}$ supported by nutrients in the ocean in this region. Our results suggested that high-turbidity ice will play an important role as a source of nutrients in the future Arctic, and that understanding its distribution, amount, and geochemical characteristics is vital.

## Data accessibility statement

The data used in this study are available in the supplementary information and archived in the data repository of the National Institute of Polar Research, Tokyo, Japan (https://doi.org/10.17592/001.2024020901).

## Supplemental files

The supplemental file for this article can be found as follows:

Supplementary Material_Akino et al.docx. Tables S1–S2. Figures S1–S3.

## Acknowledgments and funding

The authors thank the crew, technicians, and scientists of the R/V *Mirai* for their dedication to the fieldwork. Dr Takeshi Kinase assisted with sampling. This study was supported by the Japan Society for the Promotion of Science (grant numbers: JP18H03745; JP18KK0292; JP17KK0083; JP17H04715; and JP20H04345), the Joint Research Program of the Japan Arctic Research Network Center, and the Arctic Challenge for Sustainability II (ArCS II) Project.

## Competing interests

The authors declare that they have no known competing financial interests or personal relationships that could have appeared to influence the work reported in this article.

## Author contributions

Contributed to conception and design: RA, DN.

Contributed to acquisition of data: DN, MT, KM, MH, WE, TS, TK, MI, AM, AF.

Contributed to analysis and interpretation of data: All authors.

Drafted the article: RA, DN.

Revised the article: All authors.

Approved the submitted version for publication: All authors.

## References

**Aagaard, K**, **Weingartner, TJ**, **Danielson, SL**, **Woodgate, RA**, **Johnson, GC**, **Whitledge, TE.** 2006. Some controls on flow and salinity in Bering Strait. *Geophysical Research Letters* **33**(19): L19602. DOI: http://dx.doi.org/10.1029/2006GL026612.

**Ardyna, M**, **Hamilton, DS**, **Harmel, T**, **Lacour, L**, **Bernstein, DN**, **Laliberté, J**, **Horvat, C**, **Laxenaire, R**,

**Mills, MM**, **Dijken, G**, **Polyakov, I**, **Claustre, H**, **Mahowald, N**, **Arrigo, KR**. 2022. Wildfire aerosol deposition likely amplified a summertime Arctic phytoplankton bloom. *Communications Earth and Environment* **3**: 201. DOI: https://dx.doi.org/10.1038/s43247-022-00511-9.

**Arrigo, KR**, **Dieckmann, G**, **Gosselin, M**, **Robinson, DH**, **Fritsen, CH**, **Sullivan, CW.** 1995. High resolution study of the platelet ice ecosystem in McMurdo Sound, Antarctica: Biomass, nutrient, and production profiles within a dense microalgal bloom. *Marine Ecology Progress Series* **127**: 255–268. DOI: http://dx.doi.org/10.3354/Meps127255.

**Arrigo, KR**, **Perovich, DK**, **Pickart, RS**, **Brown, ZW**, **van Dijken, GL**, **Lowry, KE**, **Mills, MM**, **Palmer, MA**, **Balch, WM**, **Bahr, F**, **Bates, NR**, **Benitez-Nelson, C**, **Bowler, B**, **Brownlee, E**, **Ehn, JK**, **Frey, KE**, **Garley, R**, **Laney, SR**, **Lubelczyk, L**, **Mathis, J**, **Matsuoka, A**, **Mitchell, BG**, **Moore, GWK**, **Ortega-Retuerta, E**, **Pal, S**, **Polashenski, CM**, **Reynolds, RA**, **Schieber, B**, **Sosik, HM**, **Stephens, M**, **Swift, JH.** 2012. Massive phytoplankton blooms under Arctic Sea ice. *Science* **36**(6087): 1408. DOI: http://dx.doi.org/10.1126/science.1215065.

**Beman, JM**, **Chow, C-E**, **King, AL**, **Feng, Y**, **Fuhrman, JA**, **Andersson, A**, **Bates, NR**, **Popp, BN**, **Hutchins, DA.** 2010. Global declines in oceanic nitrification rates as a consequence of ocean acidification. *Proceeding of the National Academy of Sciences of the United States of America* **108**(1): 208–213. DOI: http://dx.doi.org/10.1073/pnas.1011053108.

**Brown, ZW**, **Casciotti, KL**, **Pickart, RS**, **Swift, JH**, **Arrigo, KR.** 2015. Aspects of the marine nitrogen cycle of the Chukchi Sea shelf and Canada Basin. *Deep Sea Research Part II: Topical Studies in Oceanography* **118**: 73–87. DOI: http://dx.doi.org/10.1016/j.dsr2.2015.02.009.

**Comiso, JC.** 2009. Enhanced sea ice concentrations and ice extents from AMSR-E data. *Journal of the Remote Sensing Society of Japan* **29**(1): 199–215. DOI: http://dx.doi.org/10.11440/rssj.29.199.

**Comiso, JC.** 2010. Variability and trends of the global sea ice cover, in Thomas, DN, Dieckmann, GS eds., *Sea ice*. 2nd ed. Hoboken, NJ: Wiley-Blackwell: 205–246.

**Cota, GF**, **Pomeroy, LR**, **Harrison, WG**, **Jones, EP**, **Peters, F**, **Sheldon, WM Jr**, **Weingartner, TR.** 1996. Nutrients, primary production and microbial heterotrophy in the southeastern Chukchi Sea: Arctic summer nutrient depletion and heterotrophy. *Marine Ecology Progress Series* **135**: 247–258. DOI: http://dx.doi.org/10.3354/meps135247.

**Cox, GFN**, **Weeks, WF.** 1983. Equations for determining the gas and brine volumes in sea-ice samples. *Journal of Glaciology* **29**(102): 306–316. DOI: http://dx.doi.org/10.3189/S0022143000008364.

**Croghan, CW**, **Egeghy, PP**. 2003 Sept 22–24. Methods of dealing with values below the limit of detection using SAS. Southern SAS User Group, St. Petersburg, FL.

**Deming, JW**, **Eicken, H**, **Iwahana, G.** 2020. Temperature, salinity, water isotope, and inorganic nutrient profiles of sea ice core sections collected offshore near Utqiaġvik, Alaska, USA in May 2017 and 2018. Biological and Chemical Oceanography Data Management Office (BCO-DMO). DOI: http://dx.doi.org/10.26008/1912/bco-dmo.816755.1.

**de Vernal, A**, **Hillaire-Marcel, C**, **Darby, DA.** 2005. Variability of sea ice cover in the Chukchi Sea (western Arctic Ocean) during the Holocene. *Paleoceanography* **20**(4): PA4018. DOI: http://dx.doi.org/10.1029/2005PA001157.

**Eicken, H**, **Gradinger, R**, **Gaylord, A**, **Mahoney, A**, **Rigor, I**, **Melling, H.** 2005. Sediment transport by sea ice in the Chukchi and Beaufort seas: Increasing importance due to changing ice conditions? *Deep-Sea Research II* **52**(24–26): 3281–3302. DOI: http://dx.doi.org/10.1016/j.dsr2.2005.10.006.

**Eicken, H**, **Kolatschek, J**, **Freitag, J**, **Lindemann, F**, **Kassens, H**, **Dmitrenko, I.** 2000. A key source area and constraints on entrainment for basin-scale sediment transport by Arctic Sea ice. *Geophysical Research Letters* **27**(13): 1919–1922. DOI: http://dx.doi.org/10.1029/1999GL011132.

**Frantz, CM**, **Light, B**, **Farley, SM**, **Carpenter, S**, **Lieblappen, R**, **Courville, Z**, **Orellana, MV**, **Junge, K.** 2019. Physical and optical characteristics of heavily melted "rotten" Arctic sea ice. *The Cryosphere* **13**(3): 775–793. DOI: http://dx.doi.org/10.5194/tc-13-775-2019.

**Frigstad, H**, **Andersen, T**, **Bellerby, RGJ**, **Silyakova, A**, **Hessen, DO.** 2014. Variation in the seston C:N ratio of the Arctic Ocean and pan-Arctic shelves. *Journal of Marine Systems* **129**: 214–223. DOI: http://dx.doi.org/10.1016/j.jmarsys.2013.06.004.

**Fripiat, F**, **Meiners, KM**, **Vancoppenolle, M**, **Papadimitriou, S**, **Thomas, DN**, **Ackley, SF**, **Arrigo, KR**, **Carnat, G**, **Cozzi, S**, **Delille, B**, **Dieckmann, GS**, **Dunbar, RB**, **Fransson, A**, **Kattner, G**, **Kennedy, H**, **Lannuzel, D**, **Munro, DR**, **Nomura, D**, **Rintala, J-M**, **Schoemann, V**, **Stefels, J**, **Steiner, N**, **Tison, J-L.** 2017. Macro-nutrient concentrations in Antarctic pack ice: Overall patterns and overlooked processes. *Elementa: Science of the Anthropocene* **1**: 5–13. DOI: http://dx.doi.org/10.1525/elementa.217.

**Giesen, WBJT**, **van Katwijk, MM**, **den Hartog, C.** 1990. Eelgrass condition and turbidity in the Dutch Wadden Sea. *Aquatic Botany* **37**(1): 71–85. DOI: http://dx.doi.org/10.1016/0304-3770(90)90065-S.

**Golden, KM**, **Ackley, SF**, **Lytle, VI.** 1998. The percolation phase transition in sea ice. *Science* **282**(5397): 2238–2241. DOI: http://dx.doi.org/10.1126/science.282.5397.2238.

**Gosselin, M**, **Levasseur, M**, **Wheeler, PA**, **Horner, RA**, **Booth, BC.** 1997. New measurements of phytoplankton and ice algal production in the Arctic Ocean. *Deep-Sea Research II* **44**(8): 1623–1644. DOI: http://dx.doi.org/10.1016/S0967-0645(97)00054-4.

**Granskog, MA**, **Kaartokallio, H**, **Shirasawa, K.** 2003. Nutrient status of Baltic Sea ice: Evidence for control by snow-ice formation, ice permeability, and ice algae. *Journal of Geophysical Research* **108**(C8): 3253. DOI: http://dx.doi.org/10.1029/2002JC001386.

**Griewank, PJ**, **Notz, D.** 2013. Insights into brine dynamics and sea ice desalination from a 1-D model study of gravity drainage. *Journal of Geophysical Research: Oceans* **118**(7): 3370–3386. DOI: http://dx.doi.org/10.1002/jgrc.20247.

**Guerrero, MA**, **Jones, RD.** 1996a. Photoinhibition of marine nitrifying bacteria. I. Wavelength-dependent response. *Marine Ecology Progress Series* **141**: 183–192. DOI: http://dx.doi.org/10.3354/meps141183.

**Guerrero, MA**, **Jones, RD.** 1996b. Photoinhibition of marine nitrifying bacteria. II. Dark recovery after monochromatic or polychromatic irradiation. *Marine Ecology Progress Series* **141**: 193–198. DOI: http://dx.doi.org/10.3354/meps141193.

**Hansell, DA**, **Goering, JJ.** 1990. Pelagic nitrogen flux in the northern Bering Sea. *Continental Shelf Research* **10**(6): 501–519. DOI: http://dx.doi.org/10.1016/0278-4343(90)90079-2.

**Hasle, GR**, **Syvertsen, EE.** 1997. Marine diatoms, in Tomas, CR ed., *Identifying marine phytoplankton*. San Diego, CA: Academic Press: 5–385.

**Hill, V**, **Cota, G.** 2005. Spatial patterns of primary production on the shelf, slope and basin of the Western Arctic in 2002. *Deep Sea Research Part II* **52**(24–26): 3344–3354. DOI: http://dx.doi.org/10.1016/j.dsr2.2005.10.001.

**Horak, REA**, **Qin, W**, **Bertagnolli, AD**, **Nelson, A**, **Heal, KR**, **Han, H**, **Heller, M**, **Schauer, AJ**, **Jeffrey, WH**, **Armbrust, EV**, **Moffett, JW**, **Ingalls, AE**, **Stahl, DA**, **Devol, AH.** 2018. Relative impacts of light, temperature, and reactive oxygen on thaumarchaeal ammonia oxidation in the North Pacific Ocean. *Limnology and Oceanography* **63**(2): 741–757. DOI: http://dx.doi.org/10.1002/lno.10665.

**Horak, REA**, **Qin, W**, **Schauer, AJ**, **Armbrust, EV**, **Ingalls, AE**, **Moffett, JW**, **Stahl, DA**, **Devol, AH.** 2013. Ammonia oxidation kinetics and temperature sensitivity of a natural marine community dominated by Archaea. *ISME Journal* **7**(10): 2023–2033. DOI: http://dx.doi.org/10.1038/ismej.2013.75.

**Jeffries, MO**, **Krouse, HR**, **Hurst-Cushing, B**, **Maksym, T**. 2001. Snow-ice accretion and snow-cover depletion on Antarctic first-year sea-ice floes. *Annals of Glaciology* **33**: 51–60. DOI: http://dx.doi.org/10.3189/172756401781818266.

**Jeffries, MO**, **Shaw, RA**, **Morris, K**, **Veazey, AL**, **Krouse, HR.** 1994. Crystal structure, stable isotopes ($\delta^{18}O$), and development of sea ice in the Ross, Amundsen, and Bellingshausen seas, Antarctica. *Journal of Geophysical Research: Oceans* **99**(C1): 985–995. DOI: http://dx.doi.org/10.1029/93JC02057.

**Joint Global Ocean Flux Study**. 1994. Protocols for the Joint Global Ocean Flux Study core measurements. Bergen, Norway: JGOFS International Project Office.

**Kaartokallio, H.** 2001. Evidence for active microbial nitrogen transformations in sea ice (Gulf of Bothnia, Baltic Sea) in midwinter. *Polar Biology* **24**: 21–28. DOI: http://dx.doi.org/10.1007/s003000000169.

**Kanna, N**, **Toyota, T**, **Nishioka, J.** 2014. Iron and macronutrient concentrations in sea ice and their impact on the nutritional status of surface waters in the Southern Okhotsk Sea. *Progress in Oceanography* **126**: 44–57. DOI: http://dx.doi.org/10.1016/j.pocean.2014.04.012.

**Kimura, N**, **Nishimura, A**, **Tanaka, Y**, **Yamaguchi, H.** 2013. Influence of winter sea-ice motion on summer ice cover in the Arctic. *Polar Research* **32**. DOI: http://dx.doi.org/10.3402/polar.v32i0.20193.

**Kimura, N**, **Oyama, M**, **Sugimura, T.** 2022. Daily polar gridded sea ice age, version 1. Arctic Data archive System (ADS), Japan. Available at https://ads.nipr.ac.jp/dataset/A20220527-001. Accessed May 30, 2023.

**Kitidis, V**, **Laverock, B**, **McNeill, LC**, **Beesley, A**, **Cummings, D**, **Tait, K**, **Osborn, MA**, **Widdicombe, S.** 2011. Impact of ocean acidification on benthic and water column ammonia oxidation. *Geophysical Research Letters* **38**(21): L21603. DOI: http://dx.doi.org/10.1029/2011GL049095.

**Kohlbach, D**, **Graeve, M**, **Lange, BA**, **David, C**, **Peeken, I**, **Flores, H.** 2016. The importance of ice algae-produced carbon in the central Arctic Ocean ecosystem: Food web relationships revealed by lipid and stable isotope analyses. *Limnology and Oceanography* **61**(6): 2027–2044. DOI: http://dx.doi.org/10.1002/lno.10351.

**Krell, A**, **Ummenhofer, C**, **Kattner, G**, **Naumov, A**, **Evans, D**, **Dieckmann, GS**, **Thomas, DN.** 2003. The biology and chemistry of land fast ice in the White Sea, Russia—A comparison of winter and spring conditions. *Polar Biology* **26**: 707–719. DOI: http://dx.doi.org/10.1007/s00300-003-0543-7.

**Krembs, C**, **Deming, JW**, **Junge, K**, **Eicken, H.** 2002. High concentrations of exopolymeric substances in Arctic winter sea ice: Implications for the polar ocean carbon cycle and cryoprotection of diatoms. *Deep-Sea Research I* **49**(12): 2163–2181. DOI: http://dx.doi.org/10.1016/S0967-0637(02)00122-X.

**Krembs, C**, **Eicken, H**, **Deming, JW.** 2011. Exopolymer alteration of physical properties of sea ice and implications for ice habitability and biogeochemistry in a warmer Arctic. *Proceedings of the National Academy of Sciences of the United States of America* **108**(9): 3653–3658. DOI: http://dx.doi.org/10.1073/pnas.1100701108.

**Kurtz, N**, **Harbeck, J.** 2017. CryoSat-2 level-4 sea ice elevation, freeboard, and thickness, version 1. Boulder, CO: NASA National Snow and Ice Data Center Distributed Active Archive Center. DOI: http://dx.doi.org/10.5067/96JO0KIFDAS8.

**Legendre, L**, **Ackley, SF**, **Dieckmann, GS**, **Gulliksen, B**, **Horner, R**, **Hoshiai, T**, **Melnikov, IA**, **Reeburgh, WS**, **Spindler, M**, **Sullivan, CW.** 1992. Ecology of sea ice biota. *Polar Biology* **12**: 429–444. DOI: http://dx.doi.org/10.1007/BF00243114.

**Leppäranta, M**, **Manninen, T.** 1988. The brine and gas content of sea ice with attention to low salinities and high temperatures. Finnish Institute of Marine Research Internal Report 88-2. Helsinki, Finland: Finnish Institute of Marine Research. Available at http://hdl.handle.net/1834/23905. Accessed November 20, 2022.

**Mahoney, AR**, **Eicken, H**, **Fukamachi, Y**, **Ohshima, KI**, **Simizu, D**, **Kambhamettu, C**, **Rohith, MV**, **Hendricks, S**, **Jones, J.** 2015. Taking a look at both sides of the ice: Comparison of ice thickness and drift speed as observed from moored, airborne and shore-based instruments near Barrow, Alaska. *Annals of Glaciology* **56**(69): 363–372. DOI: http://dx.doi.org/10.3189/2015AoG69A565.

**Martens-Habbena, W**, **Berube, PM**, **Urakawa, H**, **de la Torre, JR**, **Stahl, DA.** 2009. Ammonia oxidation kinetics determine niche separation of nitrifying archaea and bacteria. *Nature* **461**: 976–979. DOI: http://dx.doi.org/10.1038/nature08465.

**McRoy, CP.** 1993. ISHTAR, the project: An overview of inner shelf transfer and recycling in the Bering and Chukchi Seas. *Continental Shelf Research* **13**(5–6): 473–479. DOI: http://dx.doi.org/10.1016/0278-4343(93)90091-B.

**Meiners, K**, **Gradinger, R**, **Fehling, J**, **Civitarese, G**, **Spindler, M.** 2003. Vertical distribution of exopolymer particles in sea ice of the Fram Strait (Arctic) during autumn. *Marine Ecology Progress Series* **248**: 1–13. DOI: http://dx.doi.org/10.3354/meps248001.

**Merbt, SN**, **Stahl, DA**, **Casamayor, EO**, **Martí, E**, **Nicol, GW**, **Prosser, JI.** 2012. Differential photoinhibition of bacterial and archaeal ammonia oxidation. *FEMS Microbiology Letters* **327**(1): 41–46. DOI: http://dx.doi.org/10.1111/j.1574-6968.2011.02457.x.

**National Snow and Ice Data Center**. 2023. Satellite observations of ice thickness and sea-ice concentration in March and October 2021. Available at https://n5eil01u.ecs.nsidc.org/ICEBRIDGE/RDEFT4.001/. Accessed April 21, 2023.

**Nicolaus, M**, **Perovich, DK**, **Spreen, G**, **Granskog, MA**, **von Albedyll, L**, **Angelopoulos, M**, **Anhaus, P**, **Arndt, S**, **Belter, HJ**, **Bessonov, V**, **Birnbaum, G**, **Brauchle, J**, **Calmer, R**, **Cardellach, E**, **Cheng, B**, **Clemens-Sewall, D**, **Dadic, R**, **Damm, E**, **de Boer, G**, **Demir, O**, **Dethloff, K**, **Divine, DV**, **Fong, AA**, **Fons, S**, **Frey, MM**, **Fuchs, N**, **Gabarró, C**, **Gerland, S**, **Goessling, HF**, **Gradinger, R**, **Haapala, J**, **Haas, C**, **Hamilton, J**, **Hannula, H-R**, **Hendricks, S**, **Herber, A**, **Heuzé, C**, **Hoppmann, M**, **Høyland, KV**, **Huntemann, M**, **Hutchings, JK**, **Hwang, B**, **Itkin, P**, **Jacobi, H-W**, **Jaggi, M**, **Jutila, A**, **Kaleschke, L**, **Katlein, C**, **Kolabutin, N**, **Krampe, D**, **Kristensen, SS**, **Krumpen, T**, **Kurtz, N**, **Lampert, A**, **Lange, BA**, **Lei, R**, **Light, B**, **Linhardt, F**, **Liston, GE**, **Loose, B**, **Macfarlane, AR**, **Mahmud, M**, **Matero, IO**, **Maus, S**, **Morgenstern, A**, **Naderpour, R**, **Nandan, V**, **Niubom, A**, **Oggier, M**, **Oppelt, N**, **Pätzold, F**, **Perron, C**, **Petrovsky, T**, **Pirazzini, R**, **Polashenski, C**, **Rabe, B**, **Raphael, IA**, **Regnery, J**, **Rex, M**, **Ricker, R**, **Riemann-Campe, K**, **Rinke, A**, **Rohde, J**, **Salganik, E**, **Scharien, RK**, **Schiller, M**, **Schneebeli, M**, **Semmling, M**, **Shimanchuk, E**, **Shupe, MD**, **Smith, MM**, **Smolyanitsky, V**, **Sokolov, V**, **Stanton, T**, **Stroeve, J**, **Thielke, L**, **Timofeeva, A**, **Tonboe, RT**, **Tavri, A**, **Tsamados, M**, **Wagner, DN**, **Watkins, D**, **Webster, M**, **Wendisch, M**. 2022. Overview of the MOSAiC expedition: Snow and sea ice. *Elementa: Science of the Anthropocene* **10**(1): 000046. DOI: http://dx.doi.org/10.1525/elementa.2021.000046.

**Niebauer, HJ**, **Alexander, V**, **Henrichs, SM.** 1995. A time-series study of the spring bloom at the Bering Sea ice edge I. Physical processes, chlorophyll and nutrient chemistry. *Continental Shelf Research* **15**(15): 1859–1877. DOI: http://dx.doi.org/10.1016/0278-4343(94)00097-7.

**Nishino, S**, **Kikuchi, T**, **Fujiwara, A**, **Hirawake, T**, **Aoyama, M.** 2016. Water mass characteristics and their temporal changes in a biological hotspot in the Southern Chukchi Sea. *Biogeosciences* **13**(8): 2563–2578. DOI: http://dx.doi.org/10.5194/bg-13-2563-2016.

**Nomura, D**, **McMinn, A**, **Hattori, H**, **Aoki, S**, **Fukuchi, M.** 2011. Incorporation of nitrogen compounds into sea ice from atmospheric deposition. *Marine Chemistry* **127**(1–4): 90–99. DOI: http://dx.doi.org/10.1016/j.marchem.2011.08.002.

**Nomura, D**, **Nishioka, J**, **Granskog, MA**, **Krell, A**, **Matoba, S**, **Toyota, T**, **Hattori, H**, **Shirasawa, K.** 2010. Nutrient distributions associated with snow and sediment-laden layers in sea ice of the Southern Sea of Okhotsk. *Marine Chemistry* **119**(1–4): 1–8. DOI: http://dx.doi.org/10.1016/j.marchem.2009.11.005.

**Nomura, D**, **Sahashi, R**, **Takahashi, KD**, **Makabe, R**, **Ito, M**, **Tozawa, M**, **Wongpan, P**, **Matsuda, R**, **Sano, M**, **Yamamoto-Kawai, M**, **Nojiro, N**, **Tachibana, A**, **Kurosawa, N**, **Moteki, M**, **Tamura, T**, **Aoki, S**, **Murase, H.** 2023b. Biogeochemical characteristics of brash sea ice and icebergs during summer and autumn in the Indian sector of the Southern Ocean. *Progress in Oceanography* **214**: 103023. DOI: http://dx.doi.org/10.1016/j.pocean.2023.103023.

**Notz, D**, **Worster, MG**. 2009. Desalination processes of sea ice revisited. *Journal of Geophysical Research: Oceans* **114**(C5): C05006. DOI: http://dx.doi.org/10.1029/2008JC004885.

**Petrich, C**, **Eicken, H.** 2010. Growth, structure and properties of sea ice, in Thomas, DN, Dieckmann, GS eds., *Sea ice*. 2nd ed. Hoboken, NJ: Wiley-Blackwell: 23–77.

**Pondaven, P**, **Ragueneau, O**, **Tréguer, P**, **Hauvespre, A**, **Dezileau, L**, **Reyss, JL**. 2000. Resolving the 'opal paradox' in the Southern Ocean. *Nature* **405**: 168–172. DOI: http://dx.doi.org/10.1038/35012046.

**Pringle, DJ**, **Miner, JE**, **Eicken, H**, **Golden, KM.** 2009. Pore space percolation in sea ice single crystals. *Journal of Geophysical Research: Oceans* **114**(C12): 017. DOI: http://dx.doi.org/10.1029/2008JC005145.

**Qin, W**, **Amin, SA**, **Martens-Habbena, W**, **Walker, CB**, **Urakawa, H**, **Devol, AH**, **Ingalls, AE**, **Moffett, JW**, **Armbrust, EV**, **Stahl, DA.** 2014. Marine ammonia-oxidizing archaeal isolates display obligate mixotrophy and wide ecotypic variation. *Proceedings of the National Academy of Sciences of the United States of America* **111**(34): 12504–12509. DOI: http://dx.doi.org/10.1073/pnas.1324115111.

**Roukaerts, A**, **Deman, F**, **der Linden, FV**, **Carnat, G**, **Bratkic, A**, **Moreau, S**, **Lannuzel, D**, **Dehairs, F**, **Delille, B**, **Tison, JL**, **Fripiat, F.** 2021. The biogeochemical role of a microbial biofilm in sea ice: Antarctic landfast sea ice as a case study. *Elementa: Science of the Anthropocene* **9**(1): 00134. DOI: http://dx.doi.org/10.1525/elementa.2020.00134.

**Sahashi, R**, **Nomura, D**, **Toyota, T**, **Tozawa, M**, **Ito, M**, **Wongpan, P**, **Ono, K**, **Shimizu, D**, **Naoki, K**, **Nosaka, Y**, **Tamura, T**, **Aoki, S**, **Ushio, S.** 2022. Effects of snow and remineralization processes on nutrient distributions in multi-year Antarctic landfast sea ice. *Journal of Geophysical Research: Oceans* **127**(7): e2021JC018371. DOI: http://dx.doi.org/10.1029/2021JC018371.

**Serreze, MC**, **Meier, WN.** 2019. The Arctic's Sea ice cover: Trends, variability, predictability, and comparisons to the Antarctic. *Annals of the New York Academy of Sciences* **1436**(1): 36–53. DOI: http://dx.doi.org/10.1111/nyas.13856.

**Shiozaki, T**, **Ijichi, M**, **Fujiwara, A**, **Makabe, A**, **Nishino, S**, **Yoshikawa, C**, **Harada, N.** 2019. Factors regulating nitrification in the Arctic Ocean: Potential impact of sea ice reduction and ocean acidification. *Global Biogeochemical Cycles* **33**(8): 1085–1099. DOI: http://dx.doi.org/10.1029/2018GB006068.

**Spencer, RGM**, **Aiken, GR**, **Wickland, KP**, **Striegl, RG**, **Hernes, PJ.** 2008. Seasonal and spatial variability in dissolved organic matter quantity and composition from the Yukon River basin, Alaska. *Global Biogeochemical Cycles* **22**(4): GB4002. DOI: http://dx.doi.org/10.1029/2008GB003231.

**Springer, AM**, **McRoy, CP.** 1993. The paradox of pelagic food webs in the northern Bering Sea—III. Patterns of primary production. *Continental Shelf Research* **13**(5–6): 575–599. DOI: http://dx.doi.org/10.1016/0278-4343(93)90095-F.

**Stroeve, J**, **Notz, D.** 2018. Changing state of Arctic sea ice across all seasons. *Environmental Research Letters* **13**(10): 103001. DOI: http://dx.doi.org/10.1088/1748-9326/aade56.

**Subba Rao, DV**, **Platt, T.** 1984. Primary production of Arctic waters. *Polar Biology* **3**: 191–201. DOI: http://dx.doi.org/10.1007/BF00292623.

**Suzuki, R**, **Ishimaru, T**. 1990. An improved method for the determination of phytoplankton chlorophyll using N, N-dimethylformamide. *Journal of the Oceanographical Society of Japan* **46**: 190–194. DOI: https://dx.doi.org/10.1007/BF02125580.

**Thomas, DN**, **Lara, RJ**, **Eicken, H**, **Kattner, G**, **Skoog, A.** 1995. Dissolved organic matter in Arctic multi-year sea ice during winter: Major components and relationship to ice characteristics. *Polar Biology* **15**: 477–483. DOI: http://dx.doi.org/10.1007/BF00237461.

**Thomas, DN**, **Papadimitriou, S**, **Michel, C.** 2010. Biogeochemistry of sea ice, in Thomas, DN, Dieckmann, GS eds., *Sea ice: An introduction to its physical, chemistry, biology and geology*. Hoboken, NJ: Wiley-Blackwell: 425–468.

**Tomczak, M**, **Liefrink, S.** 2005. Interannual variations of water mass volumes in the Southern Ocean. *Journal of Atmospheric & Ocean Science* **10**(1): 31–42. DOI: http://dx.doi.org/10.1080/17417530500062838.

**Tovar-Sánchez, A**, **Duarte, CM**, **Alonso, JC**, **Lacorte, S**, **Tauler, R**, **Galbán-Malagón, C.** 2010. Impacts of metals and nutrients released from melting multiyear Arctic sea ice. *Journal of Geophysical Research: Oceans* **115**(C7): C07003. DOI: http://dx.doi.org/10.1029/2009JC005685.

**Waga, H**, **Eicken, H**, **Light, B**, **Fukamachi, Y.** 2022. A neural network-based method for satellite-based mapping of sediment-laden sea ice in the Arctic. *Remote Sensing of Environment* **270**: 112861. DOI: http://dx.doi.org/10.1016/j.rse.2021.112861.

**Walsh, JJ**, **McRoy, CP**, **Coachman, LK**, **Goering, JJ**, **Nihoul, JJ**, **Whitledge, TE**, **Blackburn, TH**, **Parker, PL**, **Wirick, CD**, **Shuert, PG**, **Grebmeier, JM**, **Springer, AM**, **Tripp, RD**, **Hansell, DA**, **Djenidi, S**, **Deleersnijder, E**, **Henriksen, K**, **Lund, BA**, **Andersen, P**, **Müller-Karger, FE**, **Dean, K.** 1989. Carbon and nitrogen cycling within the Bering/Chukchi Seas: Source regions for organic matter effecting AOU demands of the Arctic Ocean. *Progress in Oceanography* **22**(4): 277–359. DOI: http://dx.doi.org/10.1016/0079-6611(89)90006-2.

**Welschmeyer, NA.** 1994. Fluorometric analysis of chlorophyll a in the presence of chlorophyll b and pheopigments. *Limnology and Oceanography* **39**(8): 1985–1992. DOI: http://dx.doi.org/10.4319/lo.1994.39.8.1985.

**Werner, I**, **Ikävalko, J**, **Schünemann, H.** 2007. Sea-ice algae in Arctic pack ice during late winter. *Polar Biology* **30**: 1493–1504. DOI: http://dx.doi.org/10.1007/s00300-007-0310-2.

**World Meteorological Organization**. 1970. WMO Sea-ice nomenclature, terminology, codes and illustrated glossary, WMO/OMM/BMO 259 TP. 145, with amendments by ETSI-I, Buenos-Aires, 2002. Secretariat of the World Meteorological Organization, Geneva.

**Yun, MS**, **Whitledge, TE**, **Kong, M**, **Lee, SH.** 2014. Low primary production in the Chukchi Sea shelf, 2009. *Continental Shelf Research* **76**(15): 1–11. DOI: http://dx.doi.org/10.1016/j.csr.2014.01.001.

**Zhang, C**, **He, J**, **Yao, X**, **Mu, Y**, **Guo, X**, **Ding, X**, **Yu, Y**, **Shi, J**, **Gao, H.** 2020. Dynamics of phytoplankton and nutrient uptake following dust additions in the

northwest Pacific. *Science of the Total Environment* **739**: 139999. DOI: http://dx.doi.org/10.1016/j.scitotenv.2020.139999.

**Zhou, J**, **Delille, B**, **Eicken, H**, **Vancoppenolle, M**, **Brabant, F**, **Carnat, G**, **Geilfus, N-X**, **Papakyriakou, T**, **Heinesch, B**, **Tison, J-L.** 2013. Physical and biogeochemical properties in landfast sea ice (Barrow, Alaska): Insights on brine and gas dynamics across seasons. *Journal of Geophysical Research: Oceans* **118**(6): 3172–3189. DOI: http://dx.doi.org/10.1002/jgrc.20232.



**How to cite this article:** Akino, R, Nomura, D, Sahashi, R, Tozawa, M, Hatta, M, Matsuno, K, Endo, W, Shiozaki, T, Kawakami, T, Ito, M, Murata, A, Fujiwara, A. 2024. Characteristics of late summer Arctic brash sea ice and its melting effect on the surface-water biogeochemistry of the Chukchi Shelf and Canada Basin. *Elementa: Science of the Anthropocene* 12(1). DOI: https://doi.org/10.1525/elementa.2023.00094

**Domain Editor-in-Chief:** Jody W. Deming, University of Washington, Seattle, WA, USA

**Associate Editor:** Mathieu Ardyna, Stanford University, Stanford, CA, USA

**Knowledge Domain:** Ocean Science

**Published:** May 27, 2024 **Accepted:** April 22, 2024 **Submitted:** June 24, 2023



ELEMENTA Science of the Anthropocene

*Elem Sci Anth* is a peer-reviewed open access journal published by University of California Press.

OPEN ACCESS